Charm Production in CC DIS at HERA

Jae D. Nam

Temple Univ.

Motivations

- Charm cross section measurement in high-Q^2 charged current (CC) DIS.
  → Constraints on $s(x, Q^2)$

- Previous measurements on strangeness of the proton.
  → CCFR/NuTeV : $\frac{\int_0^1 dx[xs+x\bar{s}]}{\int_0^1 dx[x\bar{u}+x\bar{d}]} \sim 0.5$ at $x \sim 0.1$, $Q^2 \sim 10\ GeV^2$
  → ATLAS : $\frac{s+\bar{s}}{\bar{u}+\bar{d}} \sim 1.0$ at $x = 0.023, Q^2 = 1.9\ GeV^2$

- Improved determination of strange sea quark content in the proton by DESY (right)
  - Charm production in neutrino-nucleon scattering by CCFR/NuTeV, NOMAD, CHORUS
  - $W + c$ production by CMS and ATLAS

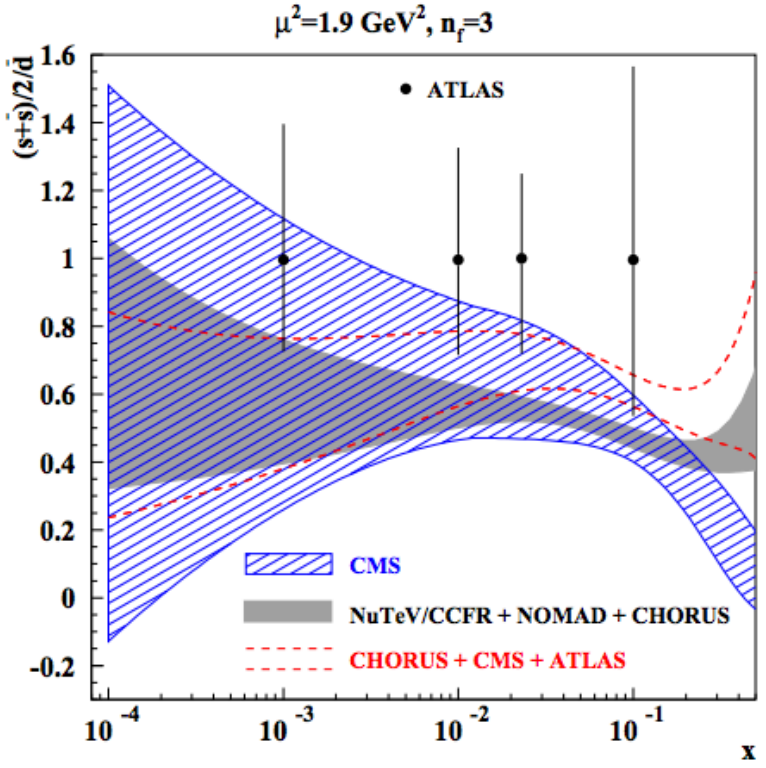

FIG. V.1: The 1σ band for the strange sea suppression factor $r_s = (s+\bar{s})/2\bar{d}$ as a function of the Bjorken x obtained in the variants of present analysis based on the combination of the data by NuTeV/CCFR [2], CHORUS [4], and NOMAD [3] (shaded area) and CHORUS [4], CMS [10], and ATLAS [11] (dashed lines), in comparison with the results obtained by the CMS analysis [10] (hatched area) and by the ATLAS *epWZ*-fit [9, 11] at different values of x (full circles). All quantities refer to the factorization scale $\mu^2 = 1.9$ GeV^2.

Charm production in CCDIS at HERA

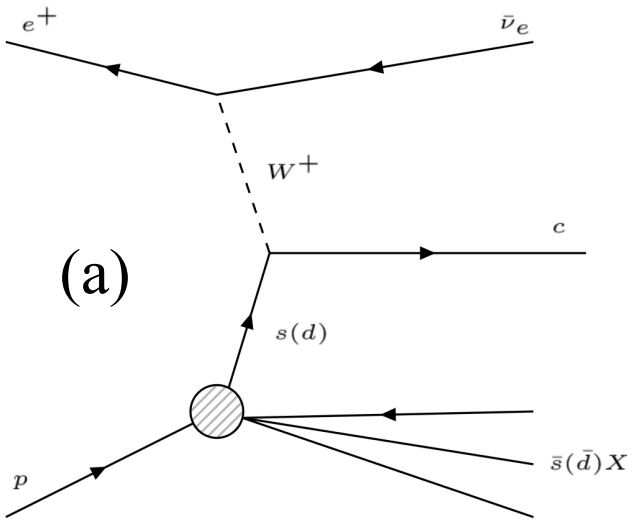

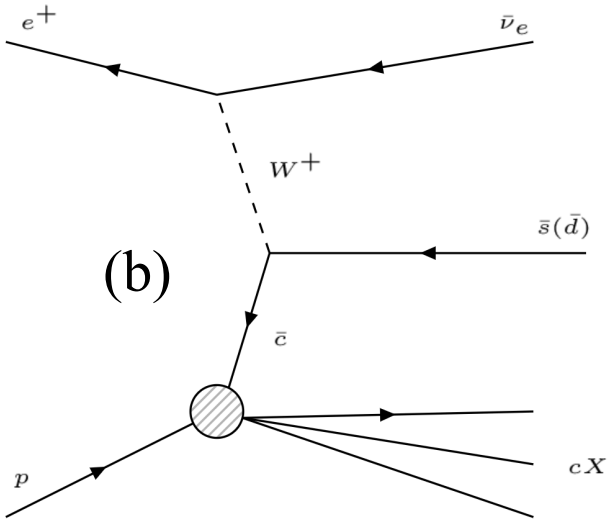

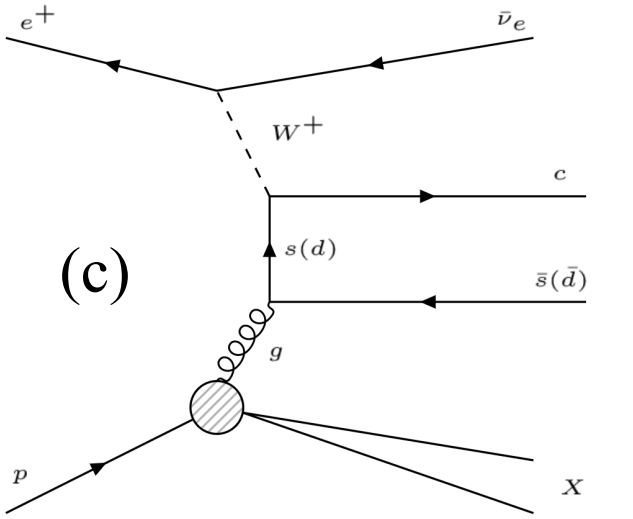

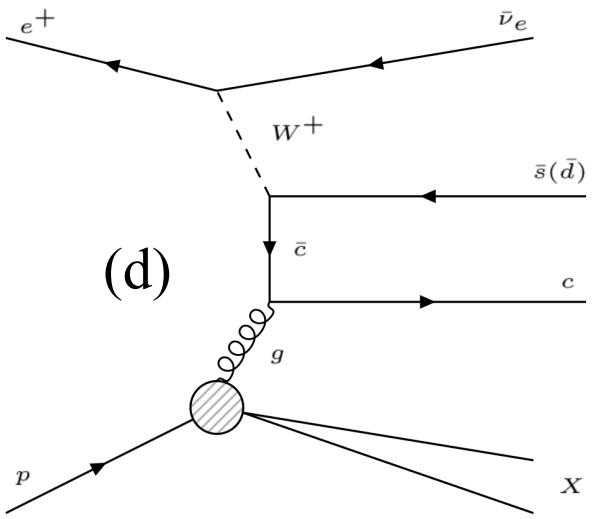

- QPM-like processes (a, b)
  - Small active charm content in the proton.
    → small contribution of (b)
  - Cabibbo-suppressed $d \rightarrow c$ transition.
  - Sensitive to the strangeness in the proton.
- BGF-like processes (c, d)
  - Sensitive to the gluon content in the proton.
- Model-dependent strange quark content extraction.

DATA & MC & Kinematic variables

Data

- HERA II ($L \cong 360\ pb^{-1}$)
  - $e^{-}p$: $05e, 06e$ w/ $L \cong 185\ pb^{-1}$
  - $e^{+}p$: $0304p, 0607p$ w/ $L \cong 173\ pb^{-1}$

Year	Collision	Integrated Luminosity (pb^{-1})
2003/04	$e^{+}p$	~ 38
2004/05	$e^{-}p$	~ 133
2006	$e^{-}p$	~ 52
2006/07	$e^{+}p$	~ 135

MC

- DIS
  - Inclusive CCDIS MC, DJANGOH 1.6, ARIADNE 4.12, CTEQ-5D.
- Background
  - Inclusive NCDIS MC: DJANGOH 1.6, ARIADNE 4.12, CTEQ-5D
  - Photoproduction MC: HERWIG, resolved & direct
  - Background contribution was found to be negligible.

- Invariant kinematic variables (x, y, Q^2) defined by using Jacquet-Blondel Method.

$$y_{JB} = \frac{\sum_h (E - p_z)_h}{2E_{e,beam}} \qquad Q^2_{JB} = \frac{p^2_{T,h}}{1 - y_{JB}} \qquad x_{JB} = \frac{Q^2_{JB}}{s y_{JB}}$$

DIS Selection Summary

General Selection	
Trigger	FLT 60 || 63 || 39 || 40 || 41 || 43 || 44 SLT EXO 4 TLT EXO 2 || EXO 6 DST 34
DQ	EVTAKE, POLTAKE, MVDTAKE, STTTAKE
p_T	p_T > 12 GeV p'_T > 10 GeV
Kinematic	200 < Q2 < 60,000 GeV2 y < 0.9
Tracking Based Selection	
Vertex	|Zvtx| < 30 cm
ϕcal - ϕtrk	dϕ < 90 degrees
Beam Gas Trk	Ntrkvtx > 0.125 * (Ntrk - 20)

**Based on 0607p CC MC by Ciesielski & Oliver

Calorimeter Based Selection	
Timing	Consistent with ep interaction
PhP, Beam Gas	Vap/Vp < 0.25 if (Pt < 20 GeV) Vap/Vp < 0.35 else
Cosmics	Reject if: Ncell < 40 or (BAC/BRMU cosmic muon) or E_RCAL > 2 GeV and f_RHAC > 0.5 or E_BCAL > 2 GeV and f_BHAC > 0.85 or f_BHAC1 > 0.7 or f_BHAC2 > 0.4 or E_FCAL > 2 GeV and f_FHAC < 0.10 or f_FHAC > 0.85 or f_FHAC1 > 0.7 or f_FHAC2 > -.6
Halo Muon	Reject if: MaxEtCell_nr <= 16384 and RCAL asosE > 0.3 GeV (FCAL) or Tsu_halo > 0 (TSUBAME in BCAL) or (BAC/BRMU halo muon)
NC DIS	Reject if: PT < 30 GeV&& E-Pz > 30 GeV && E_e > 4 GeV && E_in < 5 GeV && (Ptrk/Ee > 0.25 for 15 < θe < 164 or Ete > 2 GeV for θe > 164)

yellow – Varies between run periods
-STTTAKE = 0 for 05e data
-FLT 63 active after run 54115

green – Only applied on data
-Timing cut only on data

Control Plots – Event (e^+p)

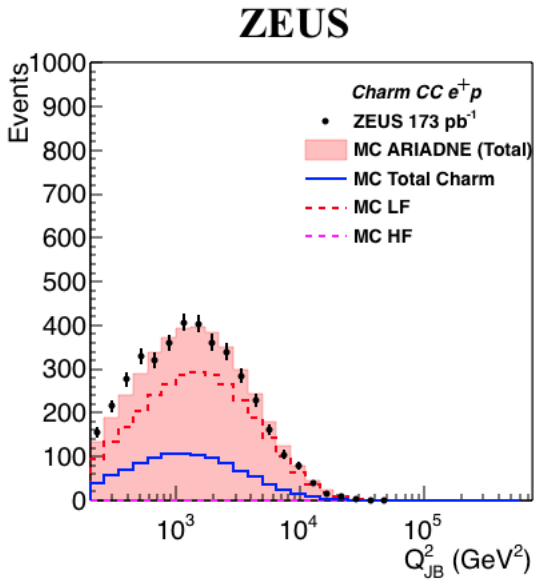

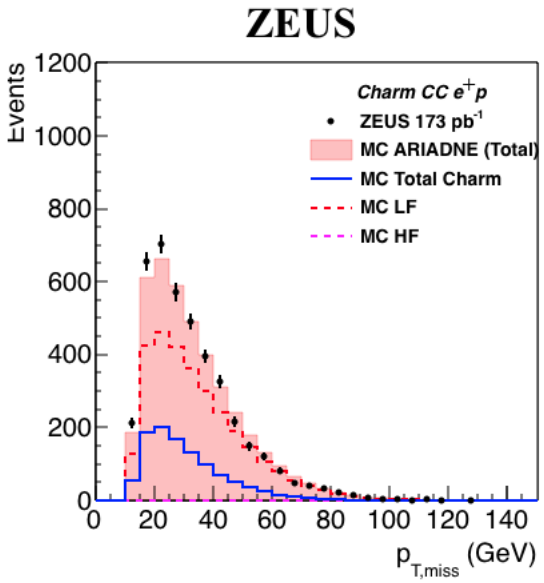

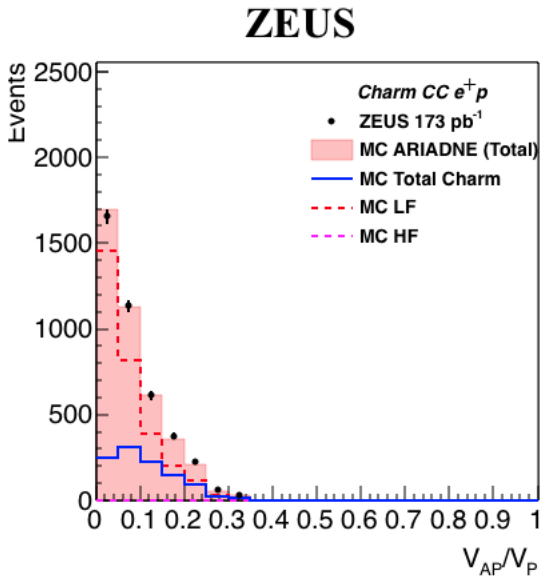

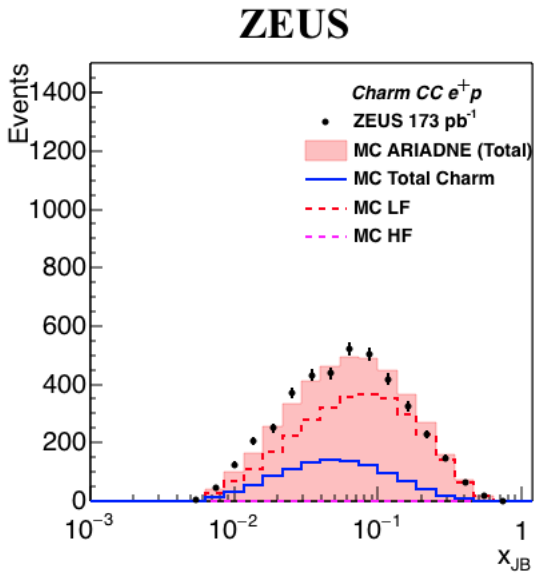

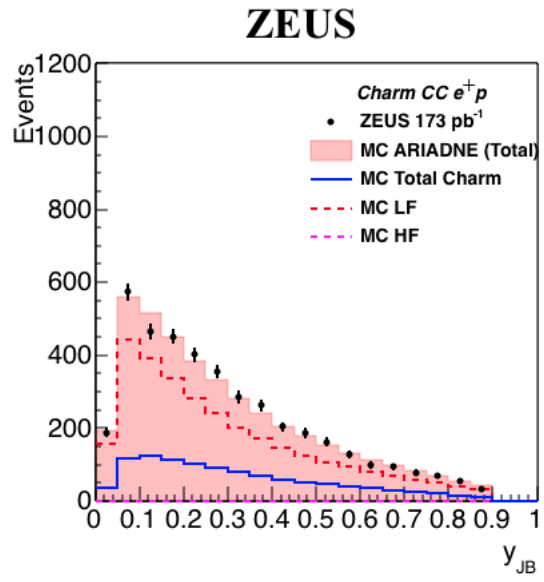

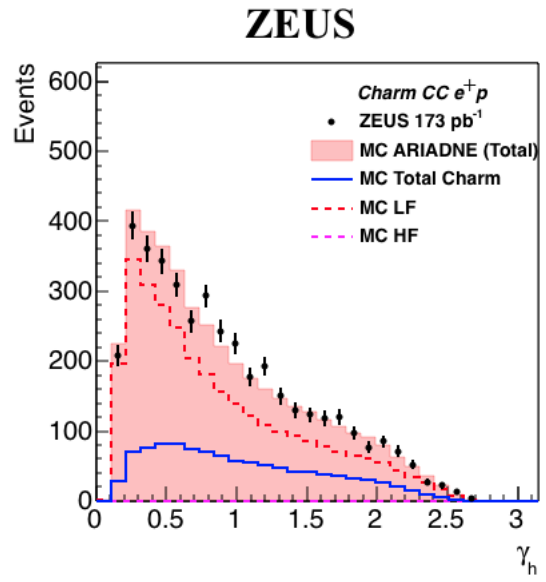

- Total charm includes all EW charm subprocesses and final state $g \rightarrow c\bar{c}$.
- Good description of data.

Control Plots – Event (e^-p)

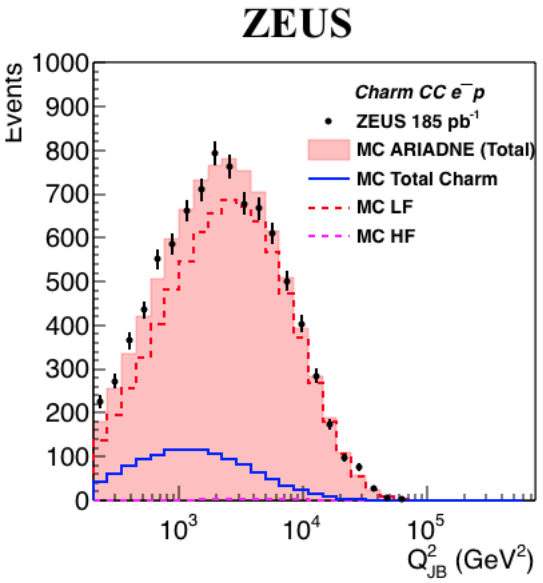

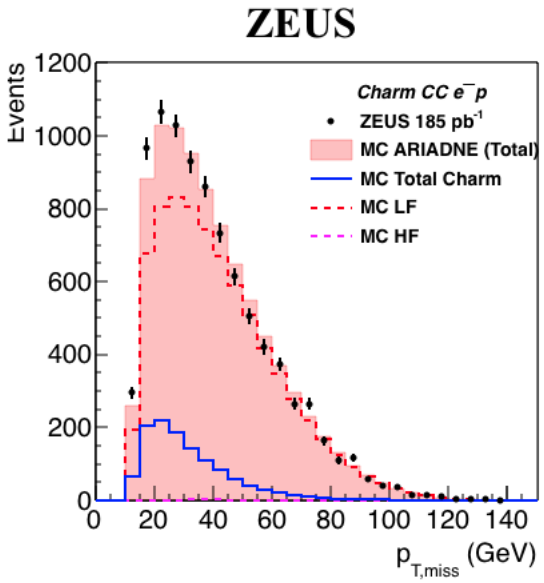

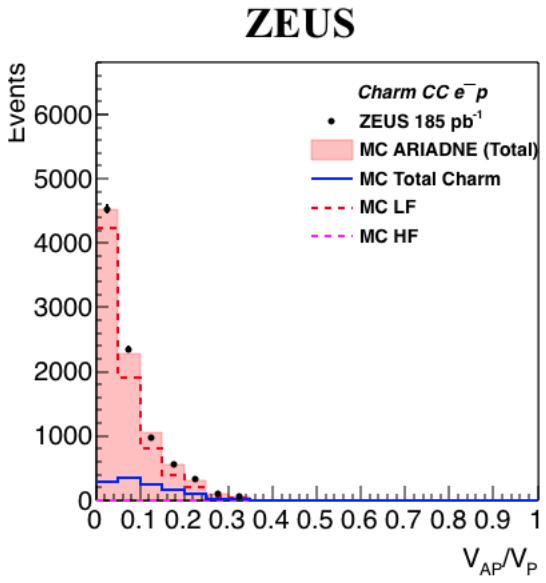

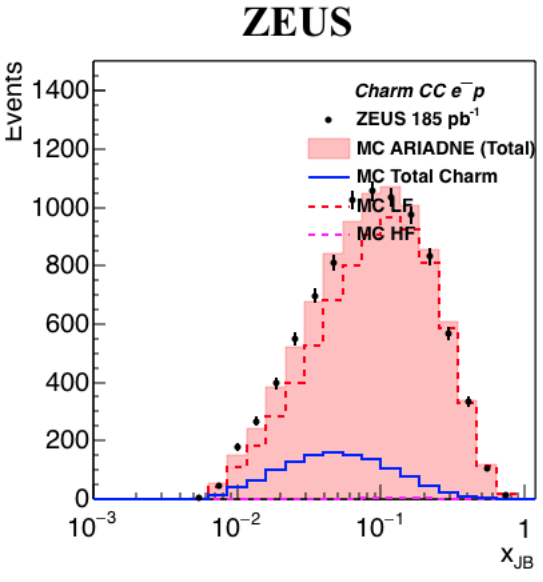

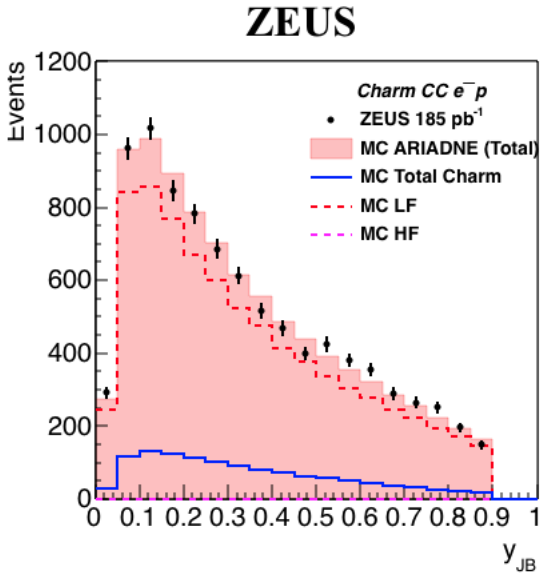

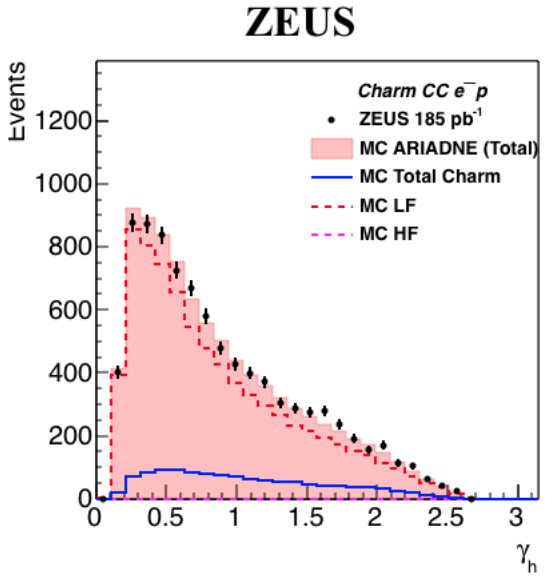

- Total 4093 and 8895 CC events selected from the e^+p and e^-p periods, respectively.
- Charm content in CCDIS is about
  - 25% in e^+p
  - 12% in e^-p

Charm Identification

Lifetime-tagging Method

- 2D decay length (L_{xy}) projected onto Jet axis.
  - LF → Short-lived, Symmetric decay length.
  - Charm → Long-lived, Asymmetric.

- LF contribution (background) suppressed by mirroring decay length distribution about $L_{xy} = 0$.

  $(N_{L+} - N_{L-}\,, N_{S+} - N_{S-})$

*S = significance

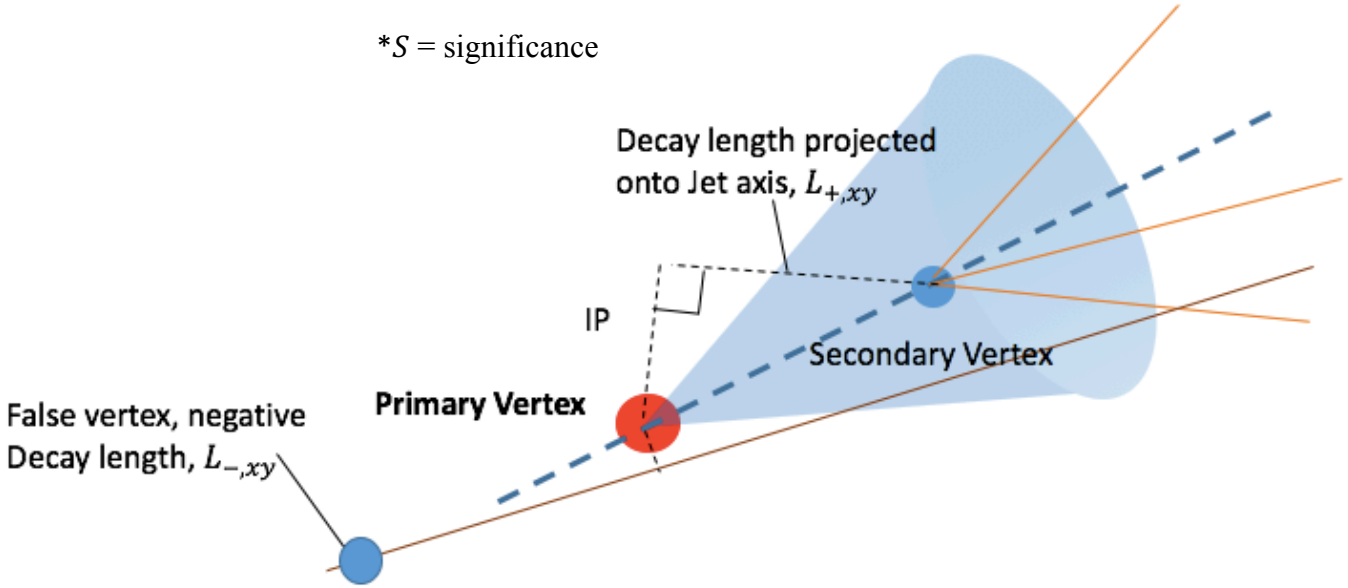

Jet Selection	Reconstructed by using kT algorithm in the massive mode.
	$E_T^{jet} > 5\ GeV$
	$-2.5 < \eta^{jet} < 2.0\ (1.5\ for\ 05e)$
SecVtx Selection	$\chi^2/N_{dof} < 6$
	$\lvert Z_{secvtx}\rvert < 30\ cm$
	Distance to beam spot $\sqrt{\Delta x^2 + \Delta y^2} < 1\ cm$
	$M_{secvtx} < 6\ GeV$
	$N_{secvtx}^{trk} > 2$

- E_T^{jet} and η^{jet} cuts further define the kinematic phase space of the measurement.

Control Plots – Jet

e^+p

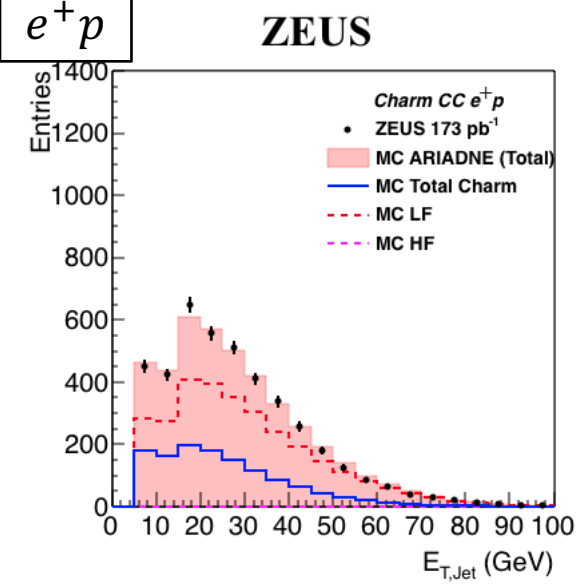

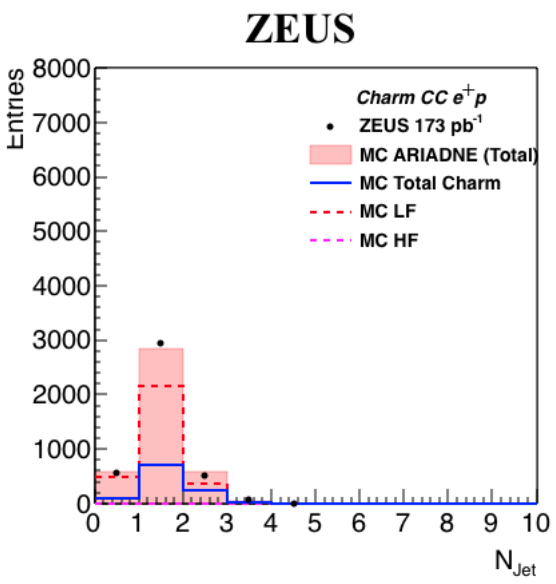

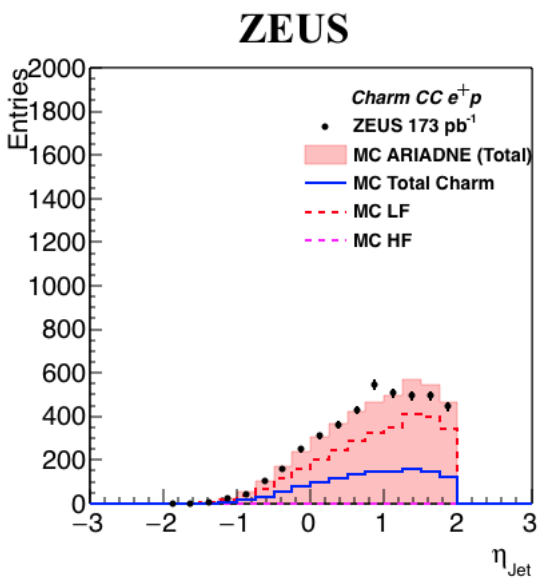

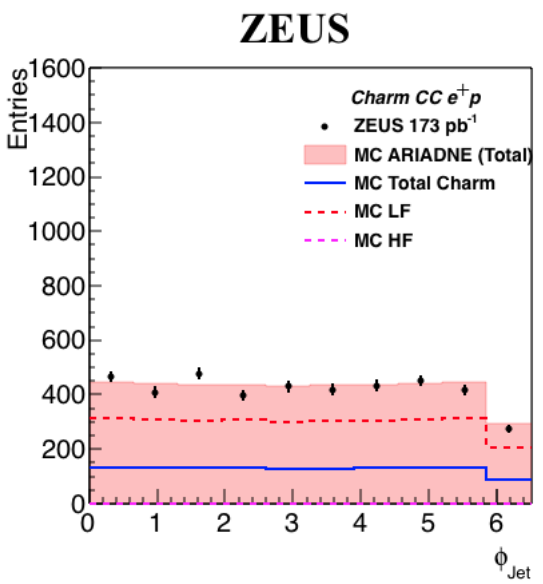

e^-p

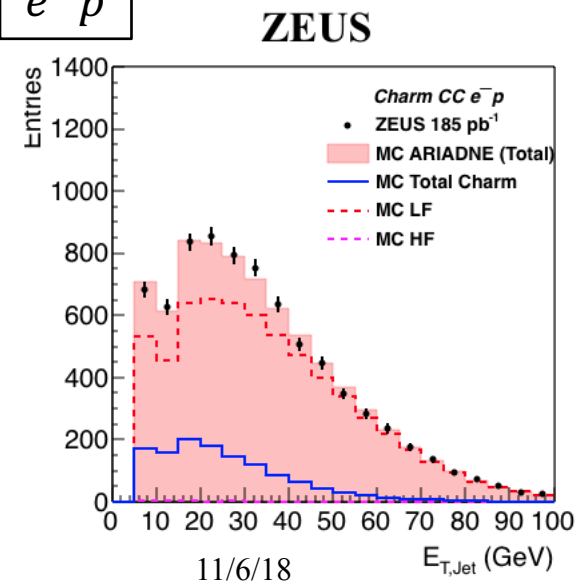

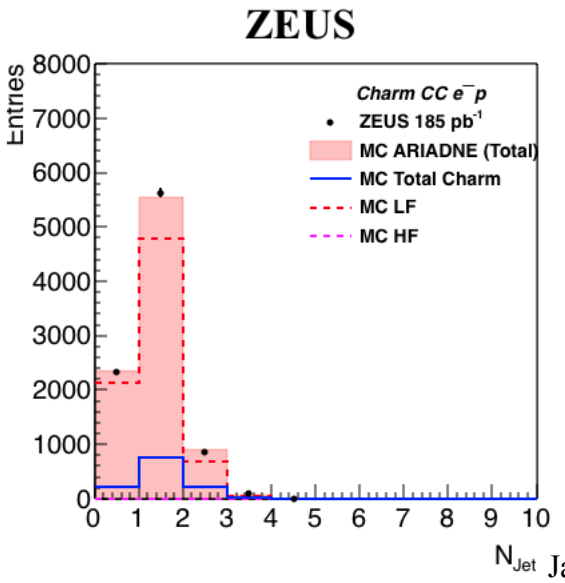

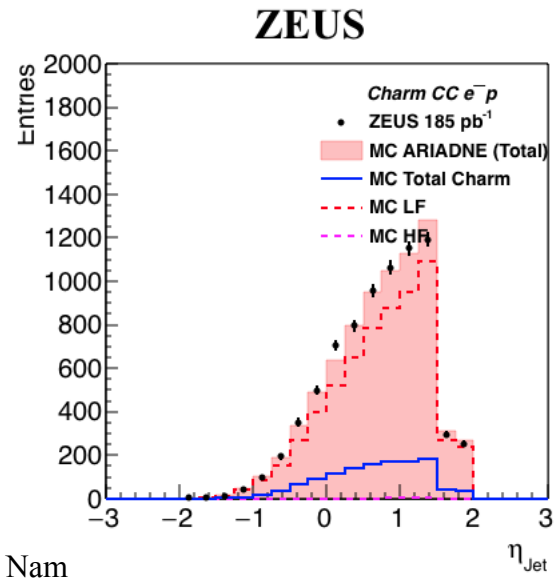

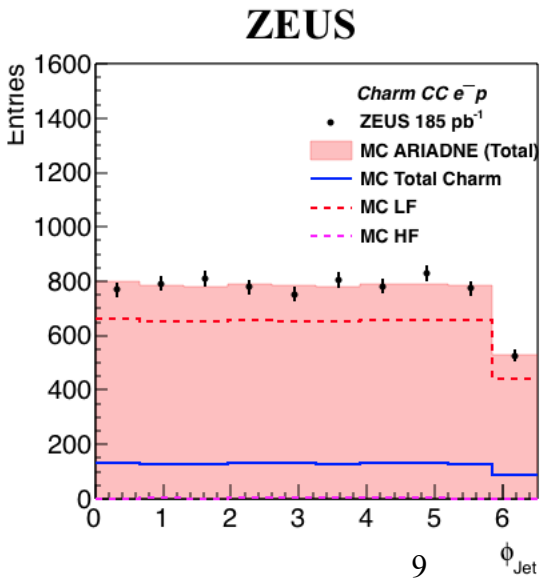

Secondary Vertex Scaling

(0607p)

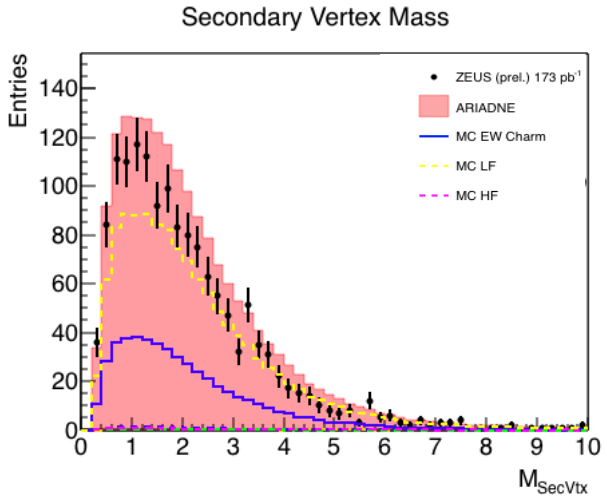

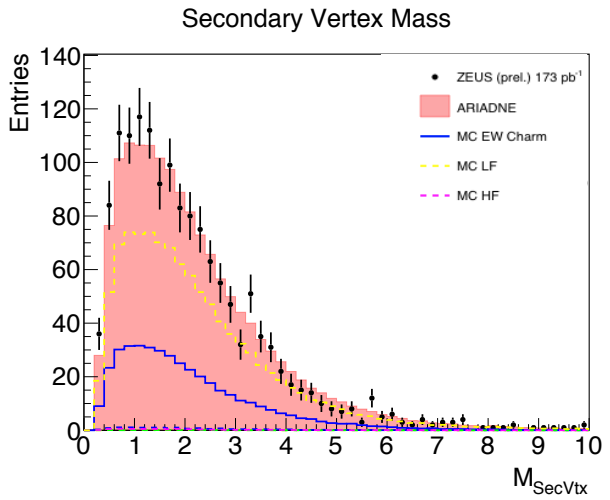

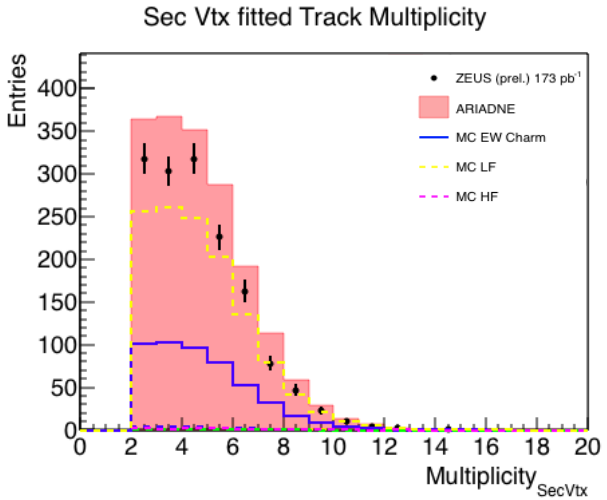

MC scaling factor
$= 0.830$

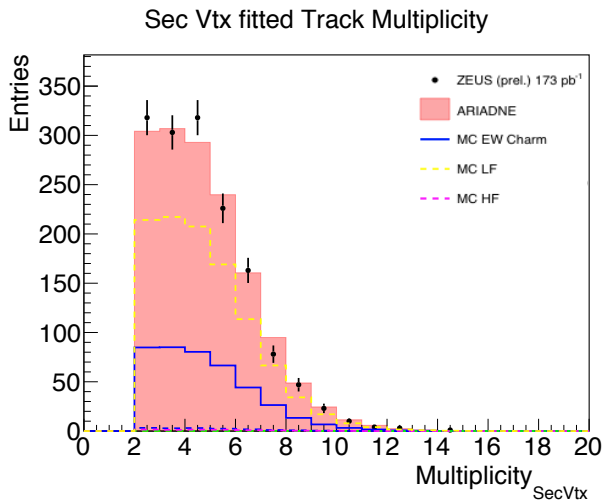

- MC overestimates trackings & secondary vertices.
- A secondary scaling applied to MC to match Data.

$$N_{SecVtx}^{DATA}/N_{SecVtx}^{MC} = 0.708 \ (0304p)$$
$$= 0.810 \ (05e)$$
$$= 0.807 \ (06e)$$
$$= 0.830 \ (0607p)$$

Control Plots – Secondary Vertex

e^+p

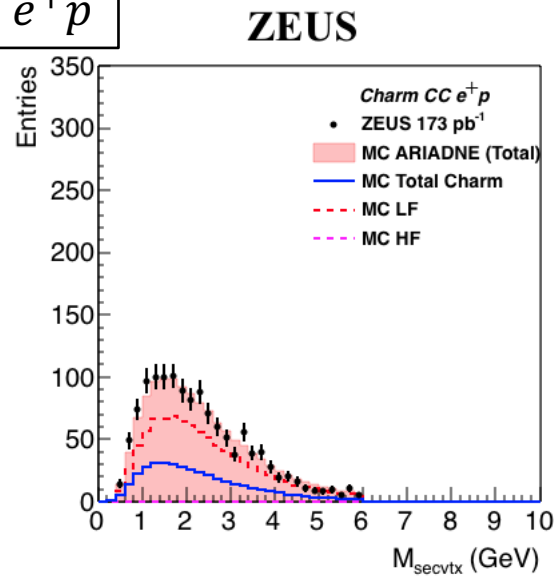

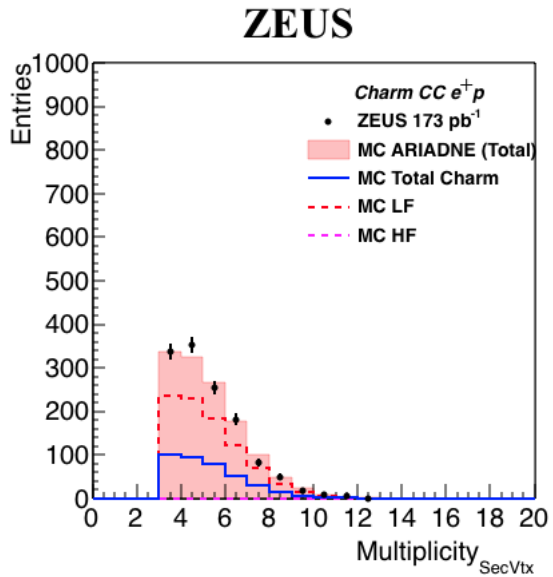

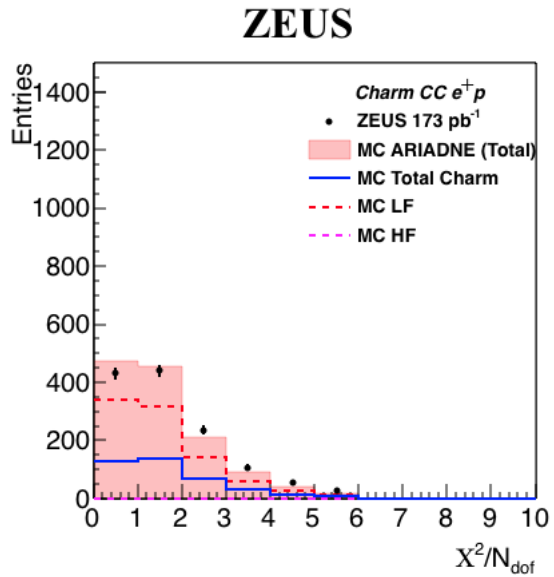

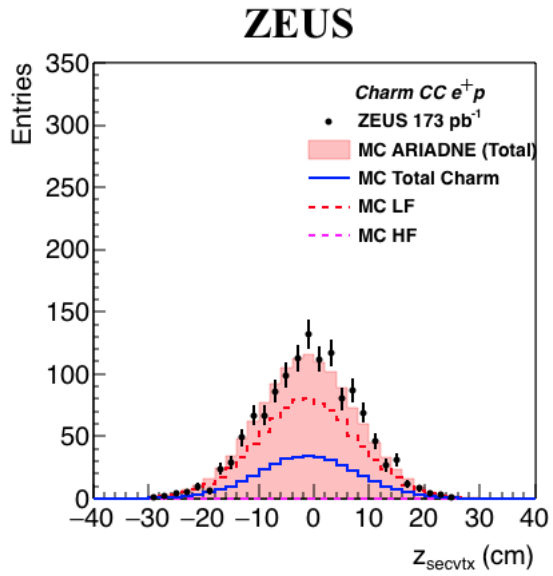

e^-p

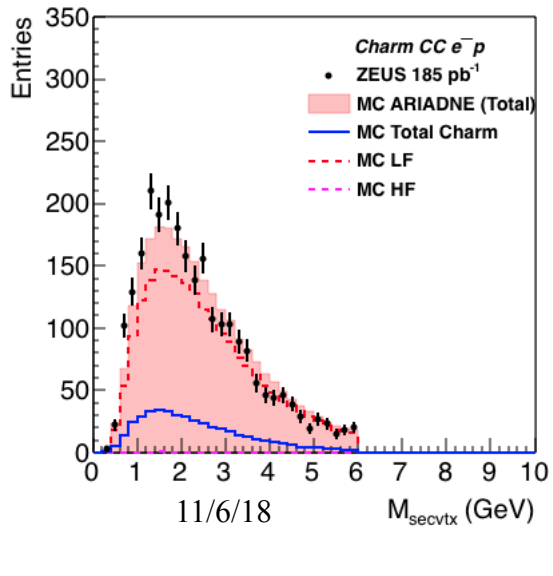

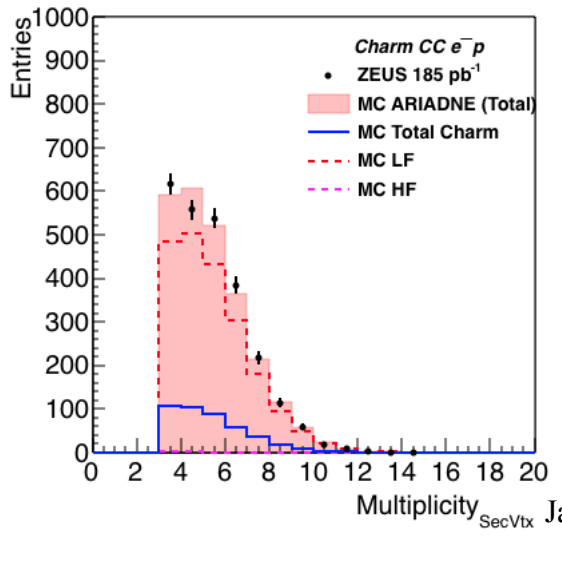

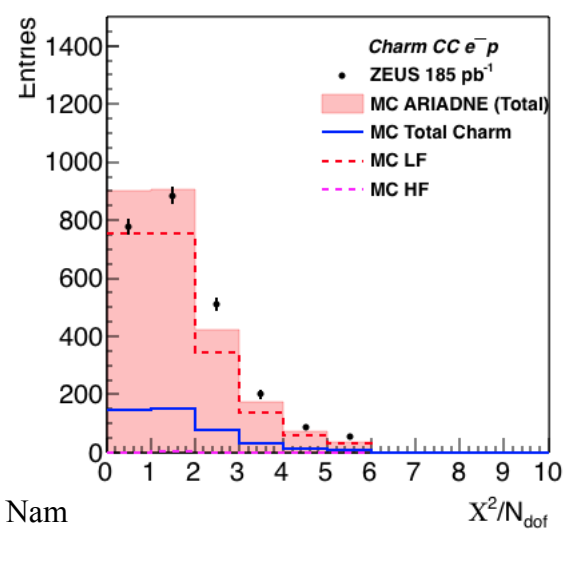

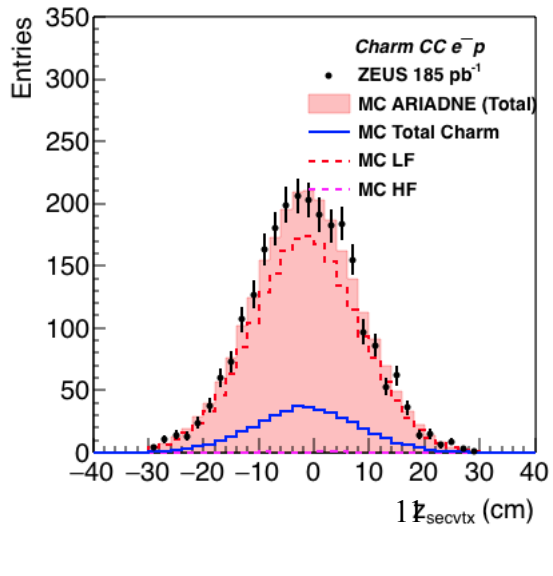

Decay Length Plots

e^+p

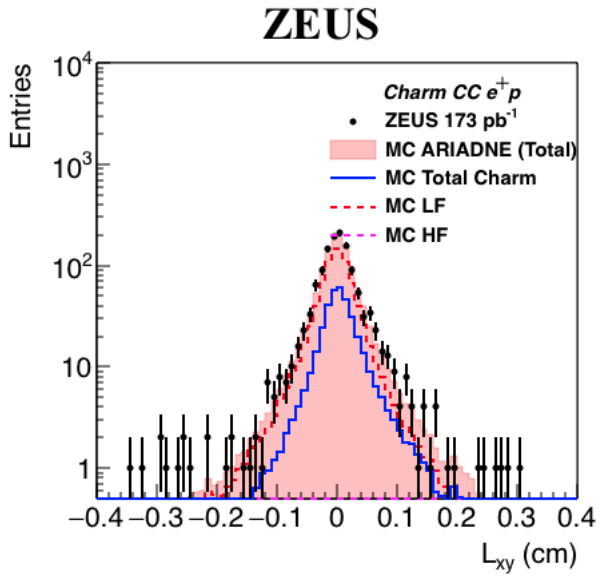

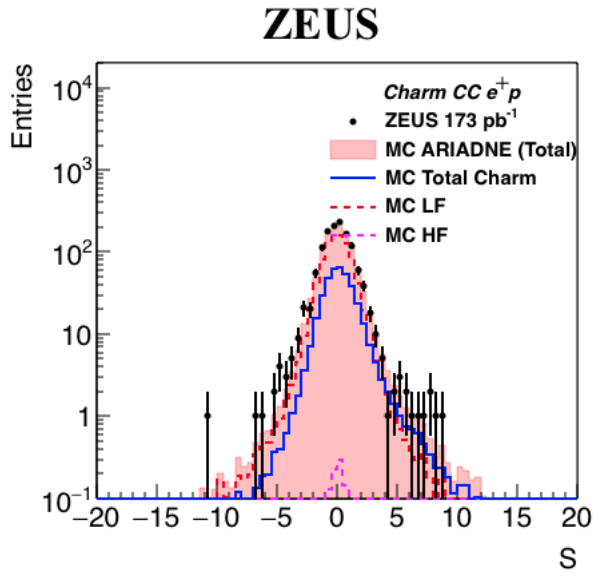

e^-p

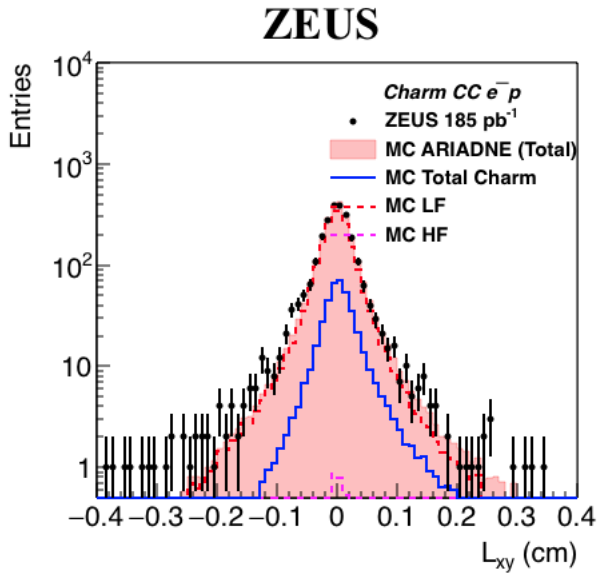

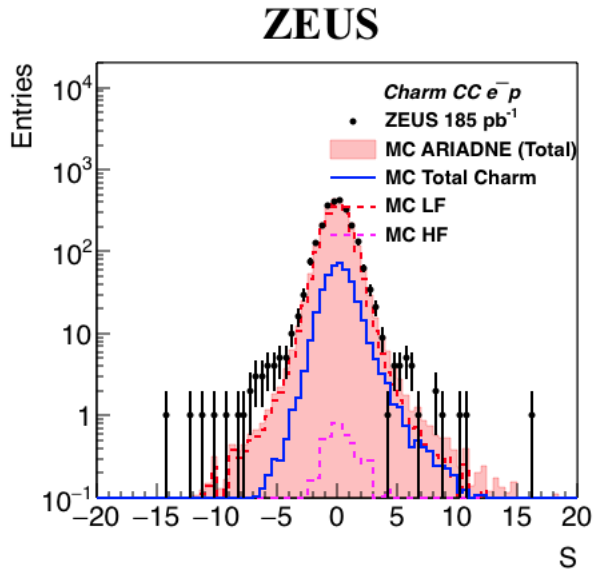

- Asymmetric charm signal observed.
- The high symmetry and large statistics around $S \sim 0$ contributes to a large statistical uncertainty in the low bin regions in $|S|$.
- A significance threshold cut $|S| > 2$ was applied to reduce overall statistical uncertainty.

Mirrored Decay Length

e^+p

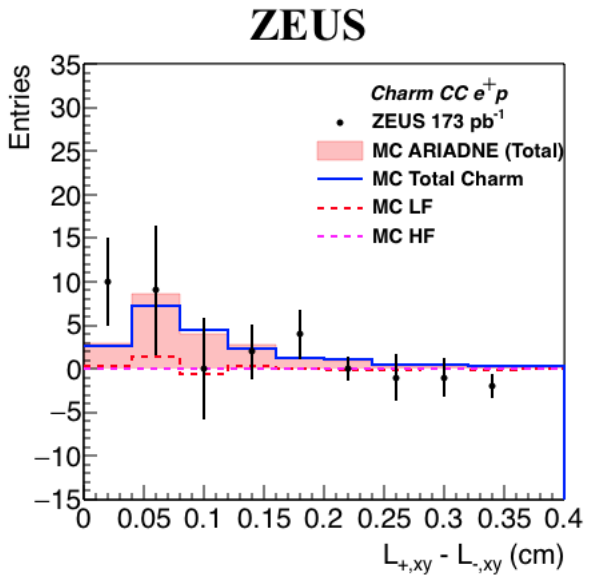

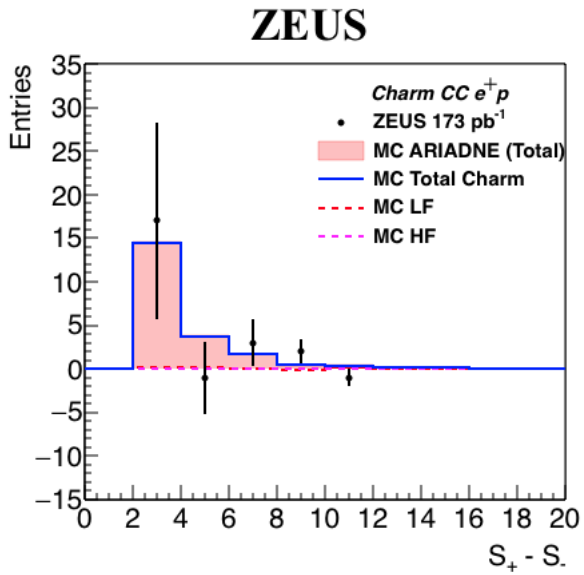

e^-p

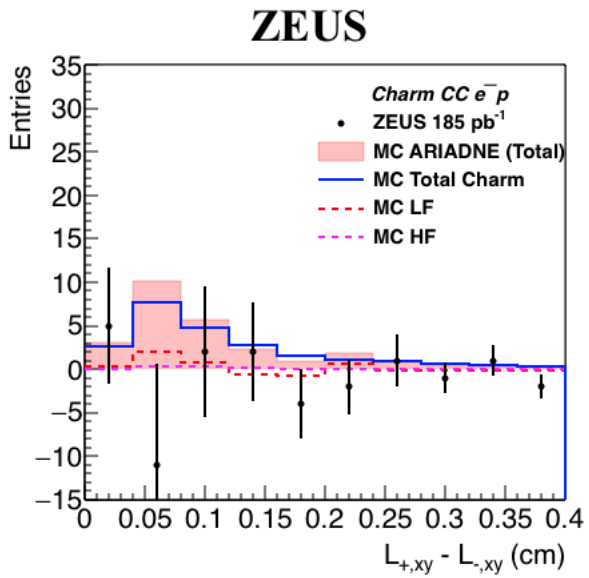

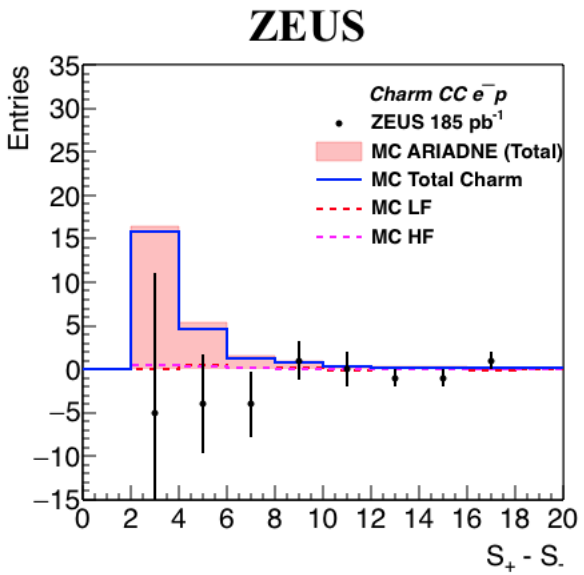

- Significance cut applied at $|S| > 2$.
- Charm signal observed with LF contribution (Background) suppressed.
- Surviving events are split into 2 bins in Q^2 to unfold charm production cross section, $\sigma_{charm,CC}$.

Charm signal & Charm generated

e^+p

M_{signal}

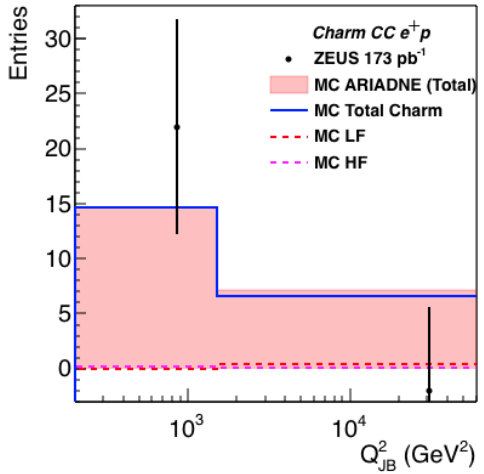

N_{kin}

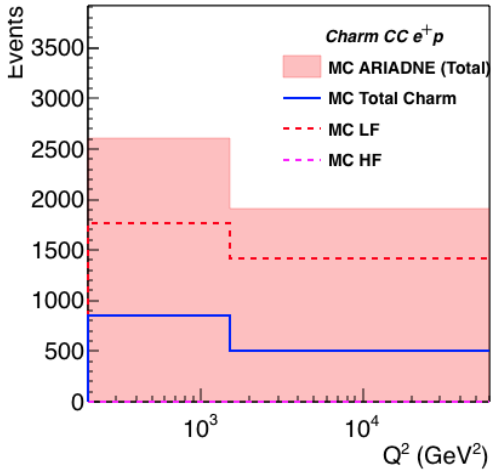

N_{gen}

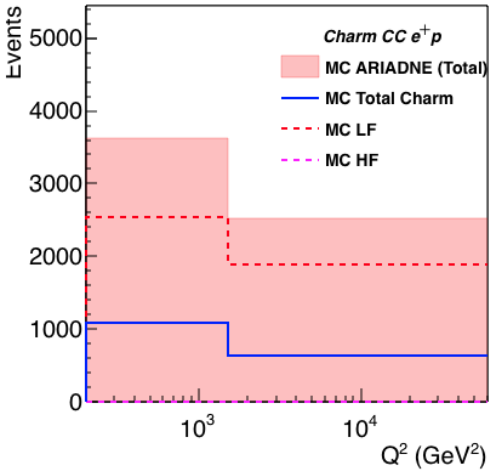

e^-p

M_{signal}

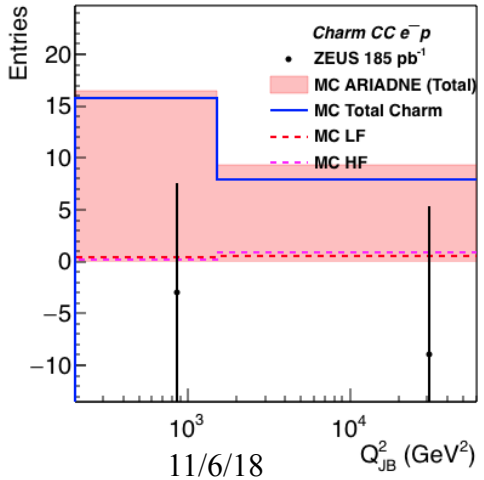

N_{kin}

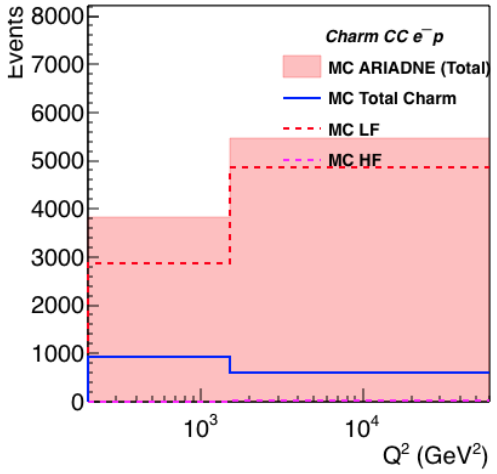

N_{gen}

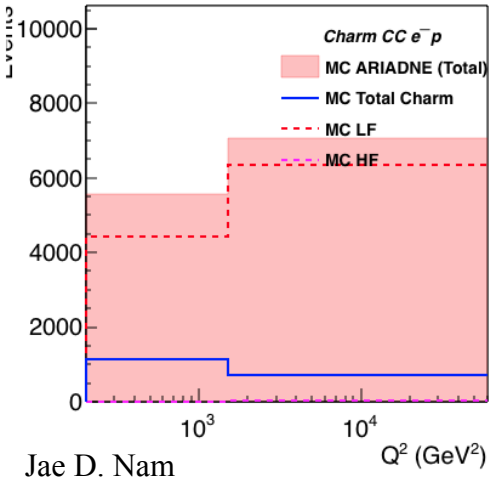

- Visible total charm cross section:

$$\sigma_{c,vis} = \frac{M^{DATA} - M_{bg}^{MC}}{M_{charm}^{MC}} \frac{N_{kin}^{MC}}{L}$$

- Visible EW charm cross section:

$$\sigma_{c^{EW},vis} = \frac{N_{EW,gen}^{MC}}{N_{gen}^{MC}} \sigma_{c,vis}$$

- Absolute EW charm cross section:

$$\sigma_{c^{EW}} = \frac{N_{gen}^{MC}}{N_{kin}^{MC}} \sigma_{c^{EW},vis}$$

Systematic Uncertainties

δ_1 DIS Selection & Secondary vertex selection

- Uncertainty associated with the selection threshold values.

δ_2 Calorimeter

- Due to imperfect calibration of hadronic calorimeter (HAC). Uncertainty in E_T^{jet} is known to be $\pm 3\%$.

δ_3 Background

- Asymmetry in LF decay length due to long-lived LF particles.

δ_4 QCD charm fraction in MC

- Uncertainty associated with the QCD charm fraction calculated in MC is tested by varying the fraction by $\pm 100\%$.

δ_4 Secondary Vertex Rescaling

- More secondary vertices survive in MC than in data. Rescaling was only applied to the light-flavor signal to account for different causes of the discrepancy.

δ_5 Signal Extraction

- Due to the low statistics & high fluctuation in data, further study will be performed.

Source	Variable	Variation	$\delta(e^+p)$ (%)	$\delta(e^-p)$ (%)
DIS	$p_T > 12\ GeV$	$> 11\ GeV$	~ 0	~ 0
		$> 13\ GeV$	-4.2	$+6.9$
	$\lvert z_{vtx}\rvert < 30\ cm$	$< 25\ cm$	$+1.4$	$+15$
		$< 35\ cm$	~ 0	~ 0
Secondary Vertex	$N_{secvtx}^{trk} > 2$	> 0	$+17$	-49
Calorimeter	$E_T^{jet} > 5\ GeV$	-3%	~ 0	$+0.9$
		$+3\%$	~ 0	~ 0
LF Background	M_{LF}	-30%	$+0.9$	$+4.4$
		$+30\%$	-0.9	-4.4
EW charm fraction	$\frac{N_{c,QCD}}{N_c}$	-100%	-0.4	-20
		$+100\%$	$+0.4$	$+18$
Rescaling	$\frac{N_{DATA}^{secvtx}}{N_{MC}^{secvtx}}$	Only on LF	-4.1	$+16$
Signal Extraction	$\lvert S\rvert > 2$	> 1	$+61$	$+63$
		> 3	-61	-63

Results

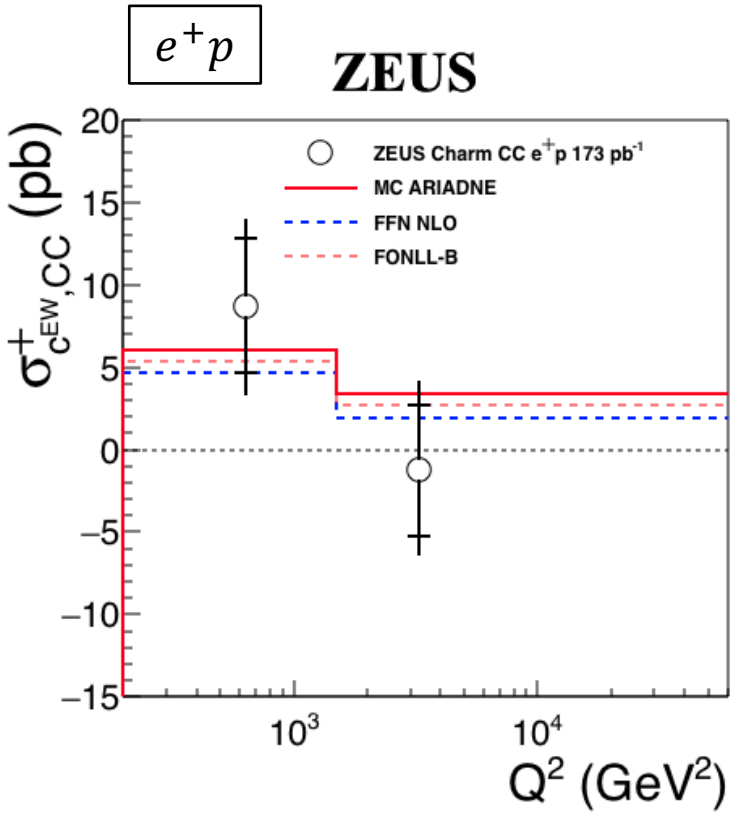

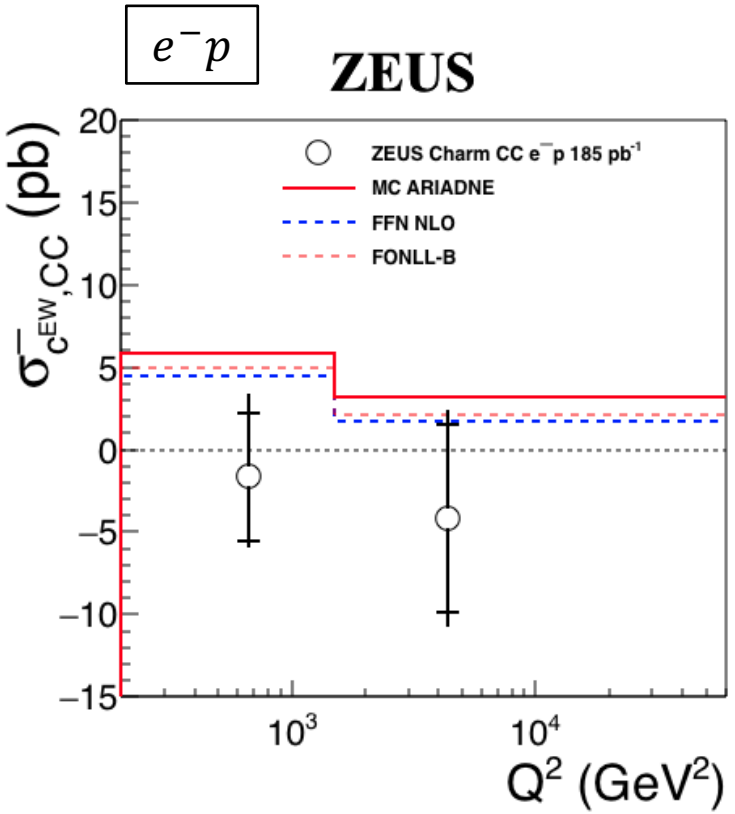

- 0304p & 0607p, 05e & 06e combined at the cross section level.
- EW charm cross sections are measured to be

$$\sigma^+_{c^{EW}} = 11.1 \pm 7.3\ (stat)\ ^{+7.1}_{-6.9}\ (syst)\ pb$$

$$\sigma^-_{c^{EW}} = -8.1 \pm 9.0\ (stat)\ ^{+6.0}_{-4.7}\ (syst)\ pb$$

- FFN scheme:
  - ABMP16.3 NLO pdf set, OPENQCDRAD
- FONLL scheme:
  - NNPDF31 NLO pdf set, APFEL
- Both are interfaced in xFitter.

Theory predictions & recap of charm subprocesses

- Charm production subprocesses are calculated in 4 different categories.

	$d \to c$	$s \to c$	$g \to c\bar{s}(\bar{d})$	$\bar{c} \to \bar{s}(\bar{d})$
MC	(a) + (c)	(a) + (c)		(b) + (d)
FFN	(a) + (c)	(a) + (c)	(d) w/ larger gluon content	
FONLL	(a) + (c)	(a) + (c)	Massive (d) – Massless (d)	(b) + Massless (d)

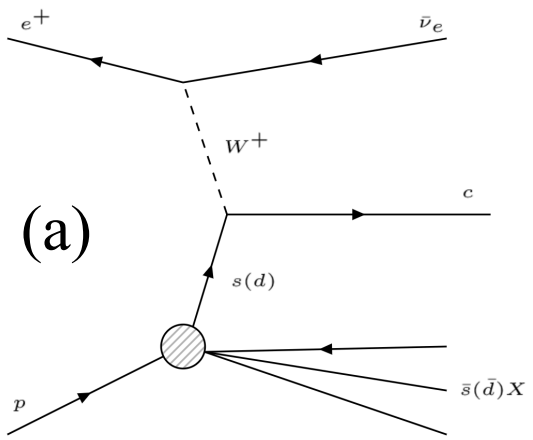

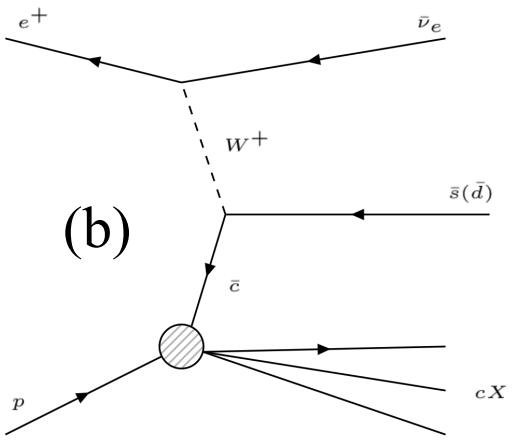

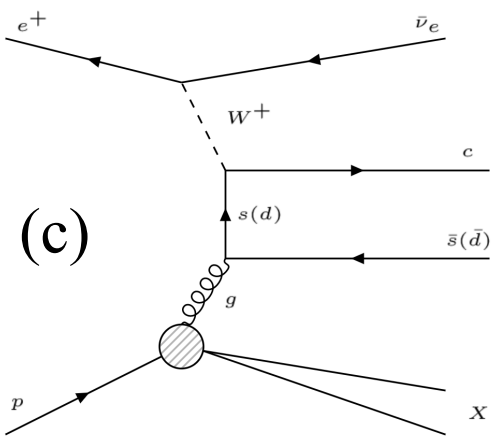

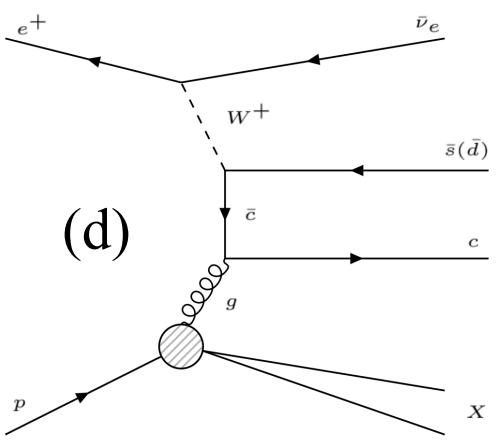

Theory predictions & recap of charm subprocesses

- First and the second columns are the QPM process in (a) $s(d) \rightarrow c$ with the BGF process in (c) $g \rightarrow s\bar{s}(d\bar{d})$ as a higher order correction.

	$d \rightarrow c$	$s \rightarrow c$	$g \rightarrow c\bar{s}(\bar{d})$	$\bar{c} \rightarrow \bar{s}(\bar{d})$
MC	(a) + (c)	(a) + (c)		(b) + (d)
FFN	(a) + (c)	(a) + (c)	(d) w/ larger gluon content	
FONLL	(a) + (c)	(a) + (c)	Massive (d) – Massless (d)	(b) + Massless (d)

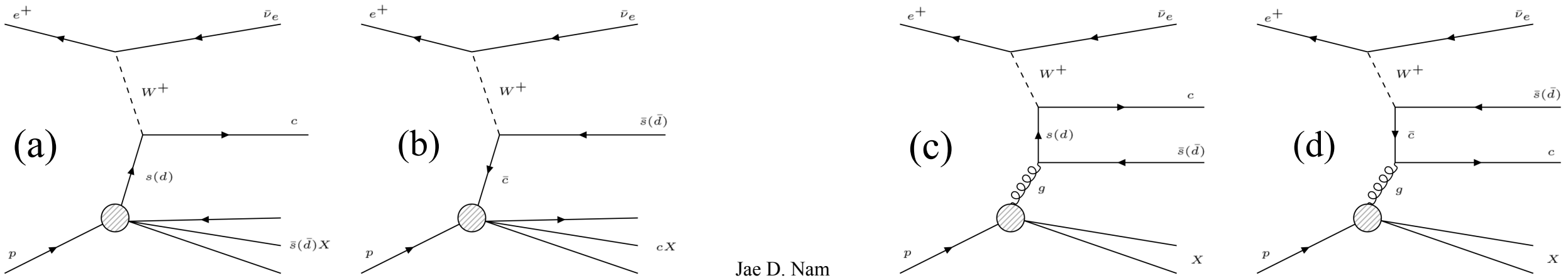

Theory predictions & recap of charm subprocesses

- Third column, for FFN scheme, is the BGF process in (d) $g \to c\bar{c}$ with a larger gluon content.
- For FONLL-B scheme, is the difference between the massive and massless calculations for process (d).

	$d \to c$	$s \to c$	$g \to c\bar{s}(\bar{d})$	$\bar{c} \to \bar{s}(\bar{d})$
MC	(a) + (c)	(a) + (c)		(b) + (d)
FFN	(a) + (c)	(a) + (c)	(d) w/ larger gluon content	
FONLL	(a) + (c)	(a) + (c)	Massive (d) – Massless (d)	(b) + Massless (d)

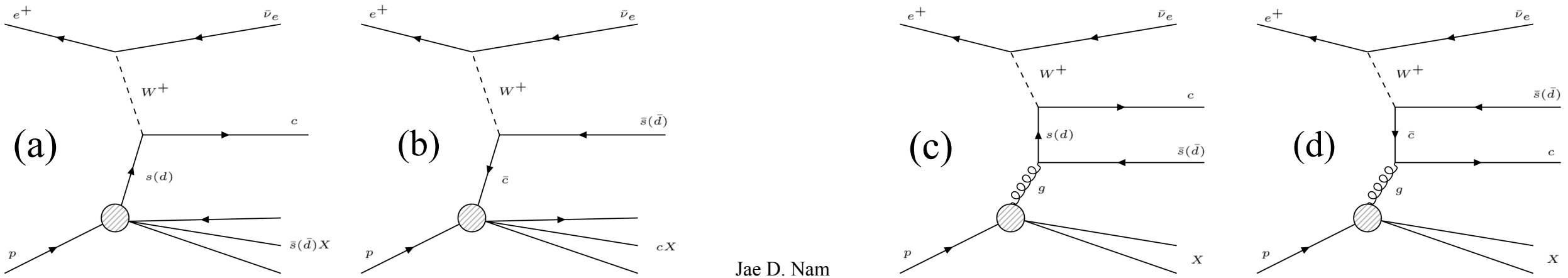

Theory predictions & recap of charm subprocesses

- Column 4 in the MC is the QPM process (b) $\bar{c} \to \bar{s}(\bar{d})$ with the BGF process (d) $g \to c\bar{c}$ as a higher order correction.
- In FONLL-B, this is (b) with the massless part of (d).

	$d \to c$	$s \to c$	$g \to c\bar{s}(\bar{d})$	$\bar{c} \to \bar{s}(\bar{d})$
MC	(a) + (c)	(a) + (c)		(b) + (d)
FFN	(a) + (c)	(a) + (c)	(d) w/ larger gluon content	
FONLL	(a) + (c)	(a) + (c)	Massive (d) – Massless (d)	(b) + Massless (d)

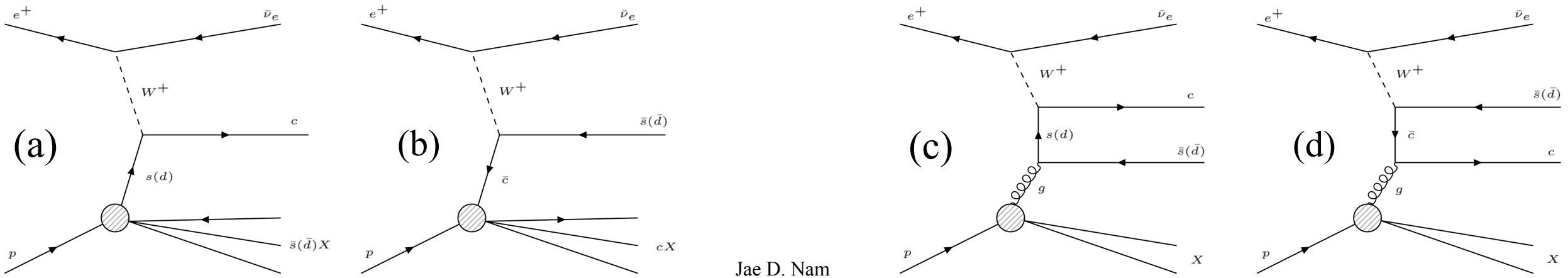

Subprocess contribution

e^+p	$200 < Q^2 < 1500\,\mathrm{GeV}^2$				
	$\sigma_{c^{EW}}$ (pb)	$d \to c(\%)$	$s \to c(\%)$	$g \to c\bar{s}/\bar{d}(\%)$	$\bar{c} \to \bar{s}/\bar{d}$
MC	6.07 ± 0.29	6	36	0	58
FFN	4.72 ± 0.05	8	49	43	0
FONLL	5.37 ± 0.21	8	43	-9	59

e^+p	$1500 < Q^2 < 60000\,\mathrm{GeV}^2$				
	$\sigma_{c^{EW}}$ (pb)	$d \to c(\%)$	$s \to c(\%)$	$g \to c\bar{s}/\bar{d}(\%)$	$\bar{c} \to \bar{s}/\bar{d}$
MC	3.42 ± 0.32	10	26	0	64
FFN	1.97 ± 0.03	16	43	41	0
FONLL	2.66 ± 0.23	12	37	-10	61

e^-p	$200 < Q^2 < 1500\,\mathrm{GeV}^2$				
	$\sigma_{c^{EW}}$ (pb)	$\bar{d} \to \bar{c}(\%)$	$\bar{s} \to \bar{c}(\%)$	$g \to \bar{c}s/d(\%)$	$c \to s/d$
MC	5.81 ± 0.40	3	37	0	60
FFN	4.50 ± 0.05	4	51	45	0
FONLL	4.98 ± 0.22	4	43	-10	64

e^-p	$1500 < Q^2 < 60000\,\mathrm{GeV}^2$				
	$\sigma_{c^{EW}}$ (pb)	$\bar{d} \to \bar{c}(\%)$	$\bar{s} \to \bar{c}(\%)$	$g \to \bar{c}s/d(\%)$	$c \to s/d$
MC	3.16 ± 0.52	2	29	0	69
FFN	1.73 ± 0.03	5	49	46	0
FONLL	2.16 ± 0.22	4	33	-12	75

Summary

- Measurements on EW Charm production in CCDIS has been performed; separately for e^+p and e^-p.
  - EW charm production has been measured within a kinematic region $200 < Q^2 < 60000\ GeV^2, y < 0.9,\ E_T^{jet} > 5\ GeV\ and\ -2.5 < \eta^{jet} < 2.0$
  - Good agreement between MC, FFN, FONLL and possibly data within the uncertainty.
  - Two major contributors are the QPM process $s \rightarrow c$ and BGF process $g \rightarrow c\bar{s}$ sharing about equal contribution.

Requested for Paper

Q^2 range (GeV^2)	$\sigma_{c^{EW}}$ (pb)				
		e^+p			
200–1500	8.7	± 4.1	(stat.)	$^{+3.4}_{-3.6}$	(syst.)
1500–60000	-1.2	± 4.0	(stat.)	$^{+3.7}_{-3.3}$	(syst.)
		e^-p			
200–1500	-2.0	± 4.0	(stat.)	$^{+3.2}_{-1.9}$	(syst.)
1500–60000	-4.4	± 5.7	(stat.)	$^{+3.3}_{-3.4}$	(syst.)

Q^2 range (GeV^2)	$\sigma_{c^{EW},vis}$ (pb)				
		e^+p			
200–1500	6.6	± 3.2	(stat.)	$^{+2.9}_{-2.9}$	(syst.)
1500–60000	-1.1	± 3.2	(stat.)	$^{+2.9}_{-2.6}$	(syst.)
		e^-p			
200–1500	-1.7	± 3.4	(stat.)	$^{+2.7}_{-1.7}$	(syst.)
1500–60000	-3.8	± 4.8	(stat.)	$^{+2.8}_{-2.9}$	(syst.)

Q^2 range (GeV^2)	$\sigma_{c,vis}$ (pb)				
		e^+p			
200–1500	6.8	± 3.3	(stat.)	$^{+3.0}_{-3.0}$	(syst.)
1500–60000	-1.1	± 3.3	(stat.)	$^{+3.1}_{-2.8}$	(syst.)
		e^-p			
200–1500	-1.7	± 3.5	(stat.)	$^{+2.8}_{-1.7}$	(syst.)
1500–60000	-4.6	± 5.9	(stat.)	$^{+3.2}_{-3.1}$	(syst.)

Requested for Paper

e^+p	$200 < Q^2 < 1500\,\mathrm{GeV}^2$				
	$\sigma_{c^{EW}}$ (pb)	$d \to c(\%)$	$s \to c(\%)$	$g \to c\bar{s}/\bar{d}(\%)$	$\bar{c} \to \bar{s}/\bar{d}$
MC	6.07 ± 0.29	6	36	0	58
FFN	4.72 ± 0.05	8	49	43	0
FONLL	5.37 ± 0.21	8	43	-9	59

e^+p	$1500 < Q^2 < 60000\,\mathrm{GeV}^2$				
	$\sigma_{c^{EW}}$ (pb)	$d \to c(\%)$	$s \to c(\%)$	$g \to c\bar{s}/\bar{d}(\%)$	$\bar{c} \to \bar{s}/\bar{d}$
MC	3.42 ± 0.32	10	26	0	64
FFN	1.97 ± 0.03	16	43	41	0
FONLL	2.66 ± 0.23	12	37	-10	61

e^-p	$200 < Q^2 < 1500\,\mathrm{GeV}^2$				
	$\sigma_{c^{EW}}$ (pb)	$\bar{d} \to \bar{c}(\%)$	$\bar{s} \to \bar{c}(\%)$	$g \to \bar{c}s/d(\%)$	$c \to s/d$
MC	5.81 ± 0.40	3	37	0	60
FFN	4.50 ± 0.05	4	51	45	0
FONLL	4.98 ± 0.22	4	43	-10	64

e^-p	$1500 < Q^2 < 60000\,\mathrm{GeV}^2$				
	$\sigma_{c^{EW}}$ (pb)	$\bar{d} \to \bar{c}(\%)$	$\bar{s} \to \bar{c}(\%)$	$g \to \bar{c}s/d(\%)$	$c \to s/d$
MC	3.16 ± 0.52	2	29	0	69
FFN	1.73 ± 0.03	5	49	46	0
FONLL	2.16 ± 0.22	4	33	-12	75

Requested for Paper

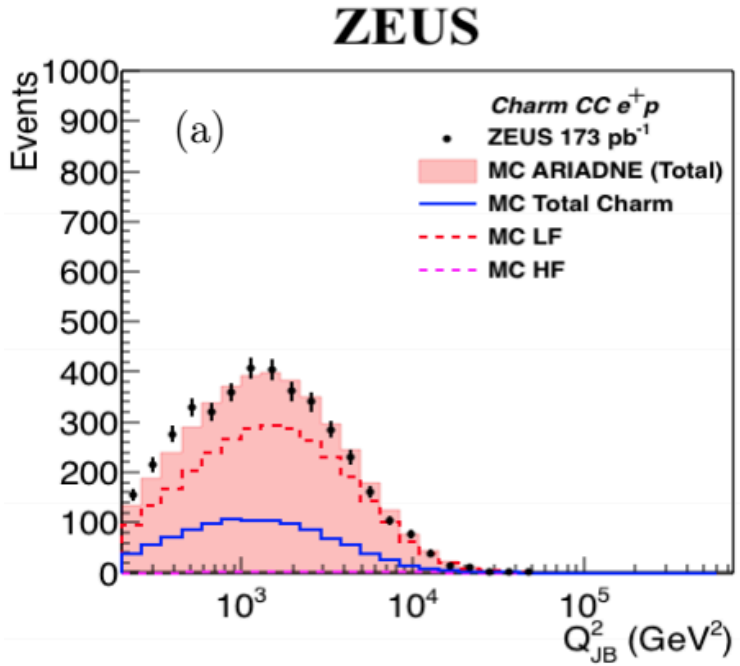

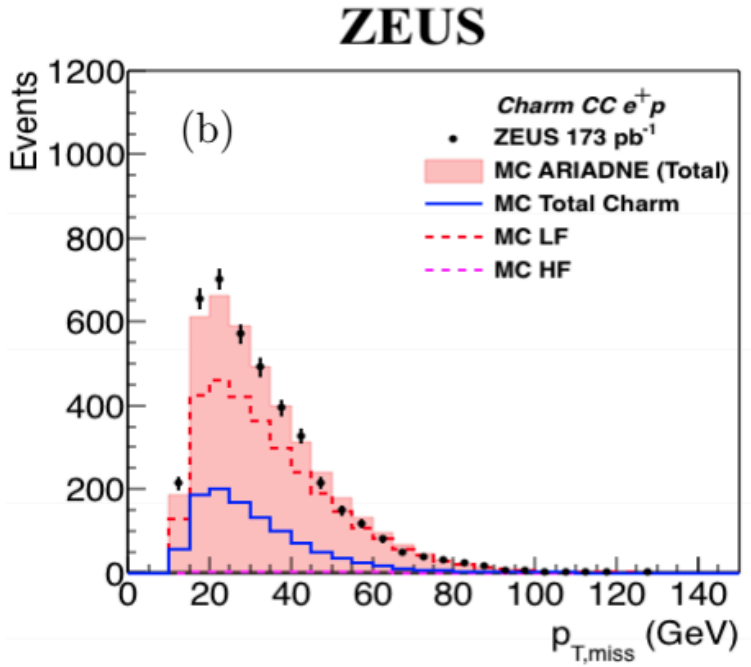

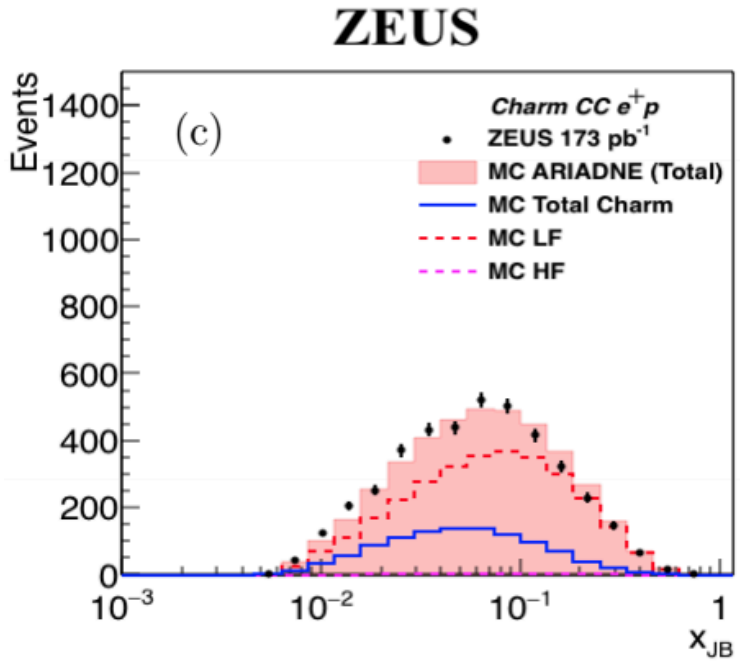

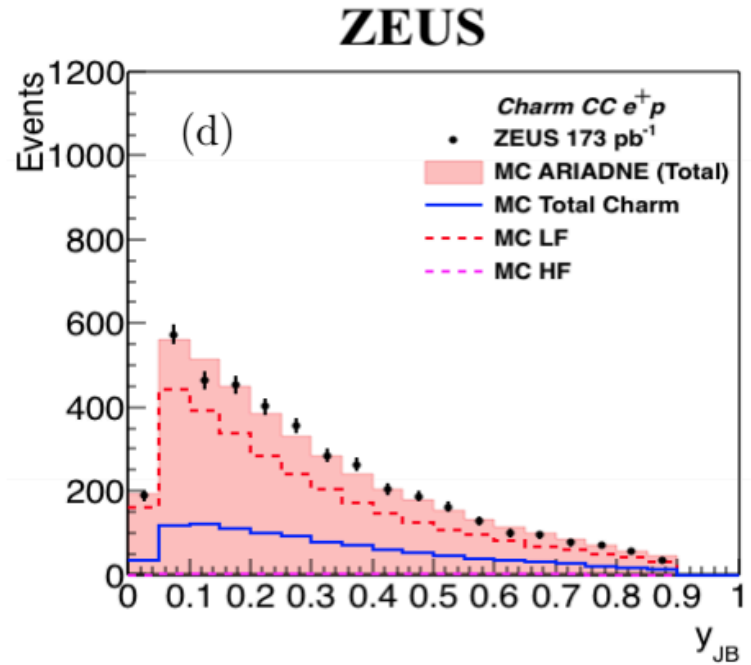

Requested for Paper

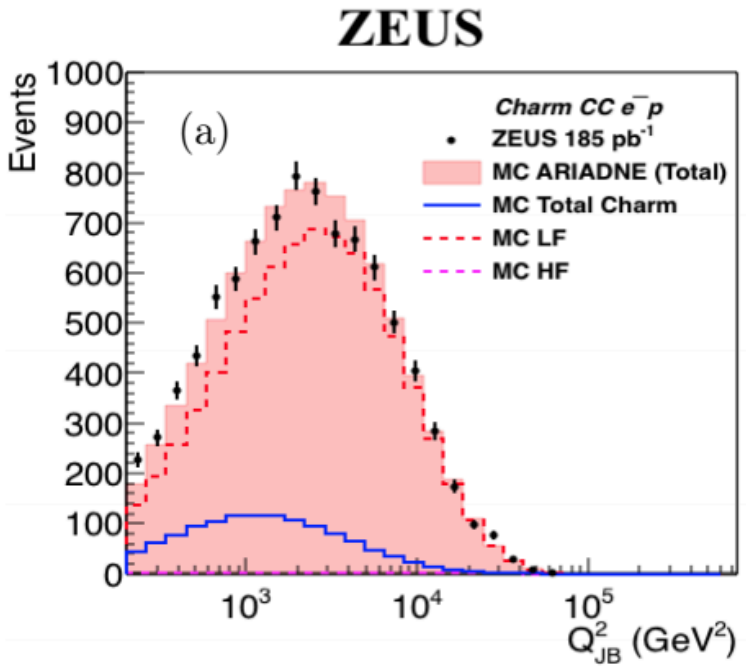

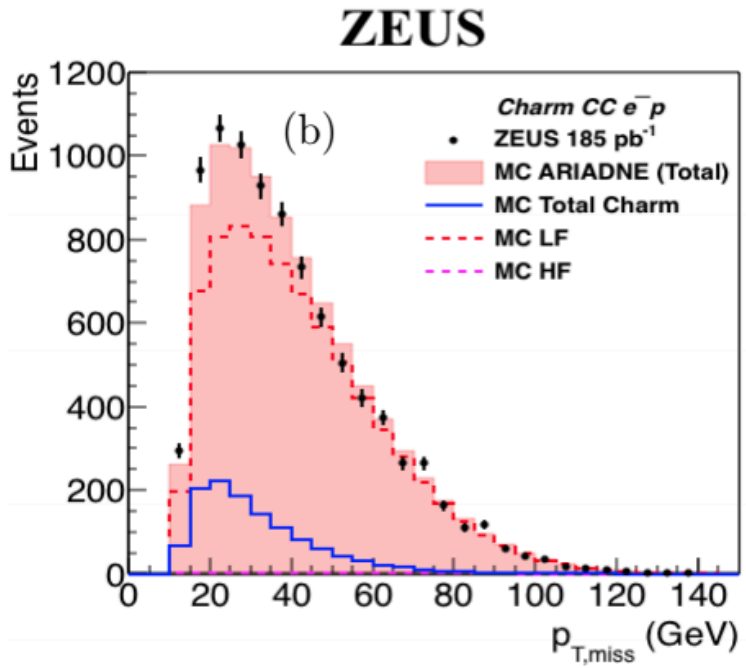

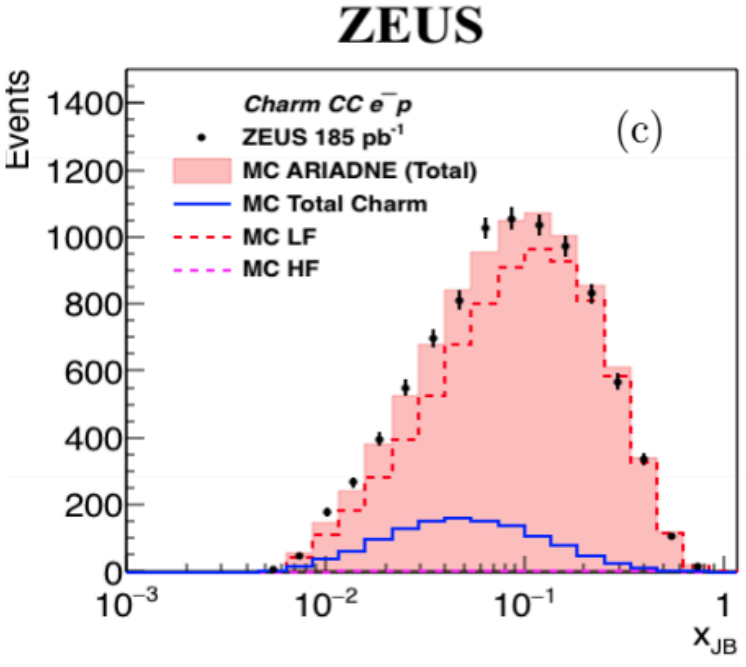

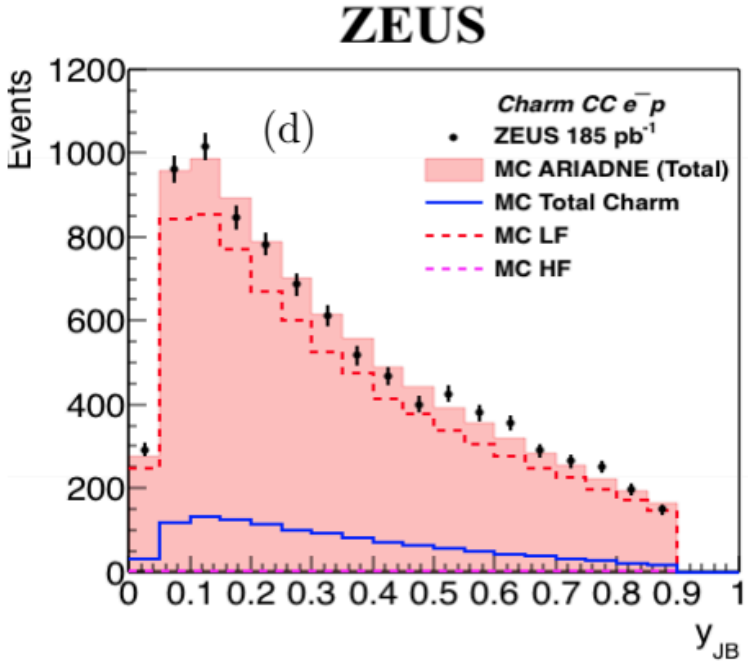

Requested for Paper

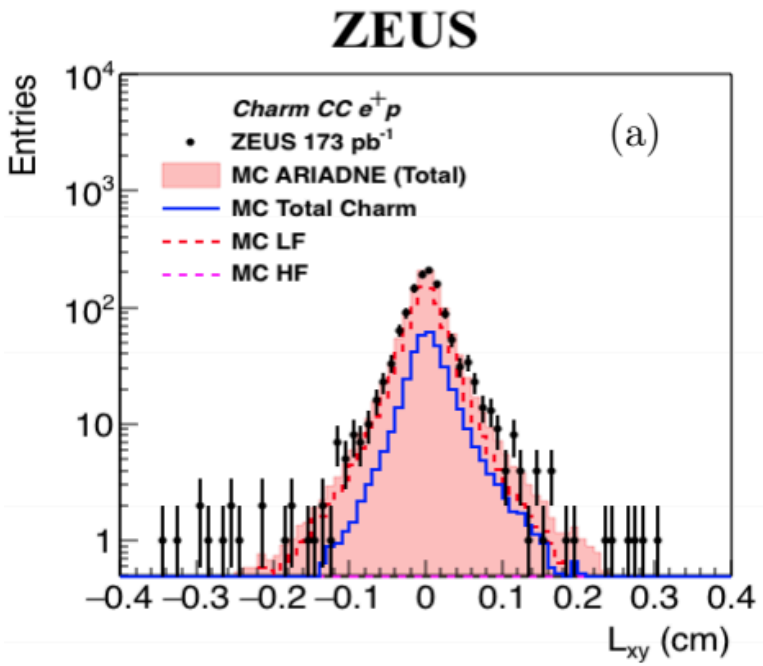

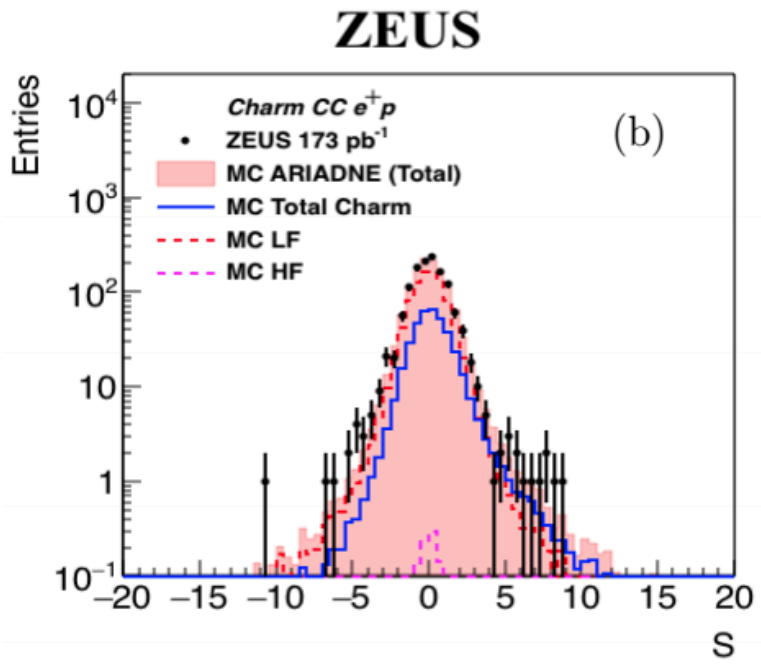

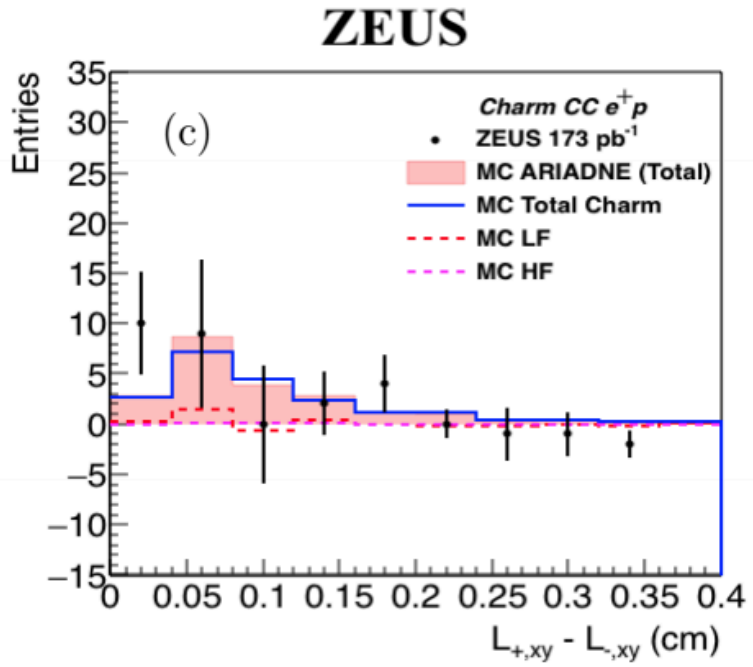

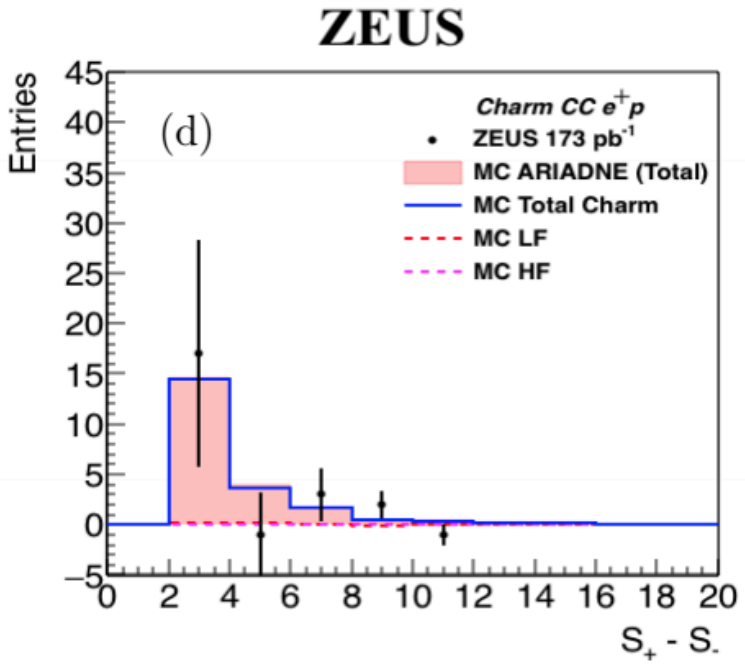

Requested for Paper

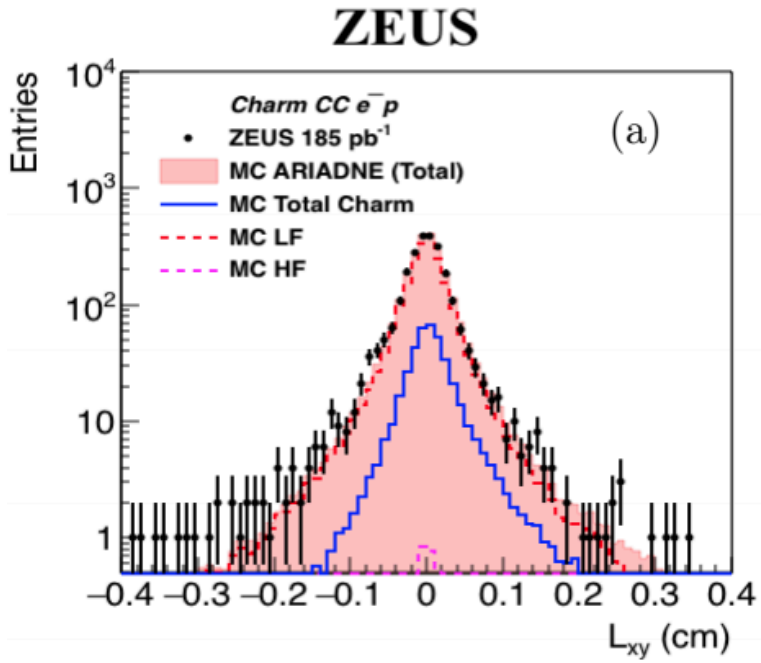

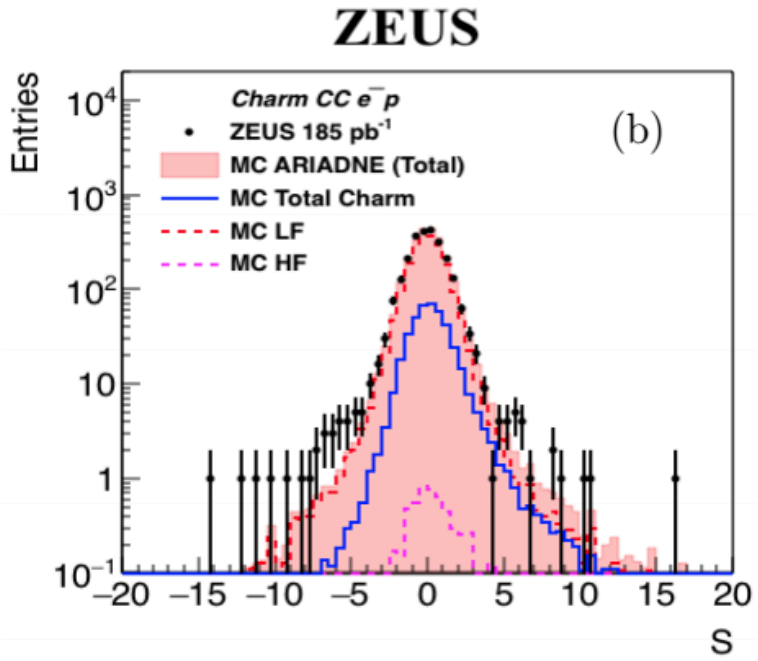

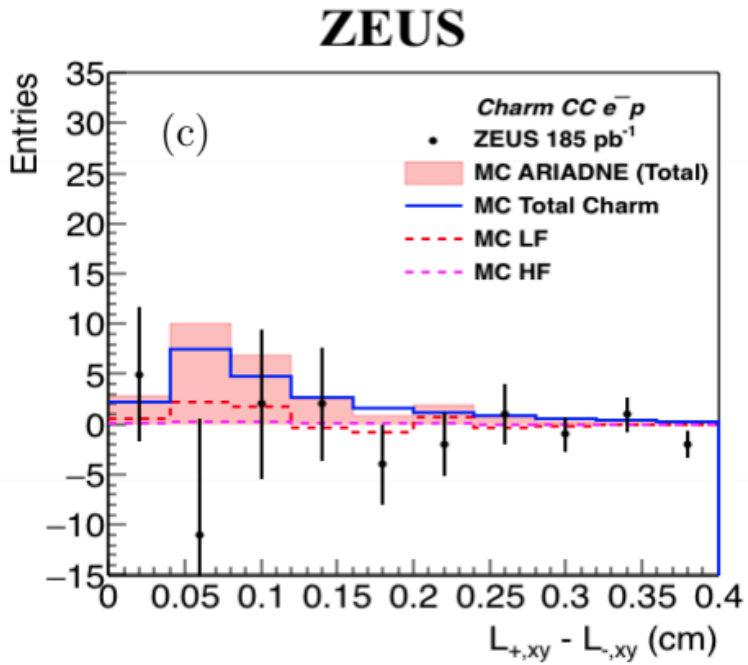

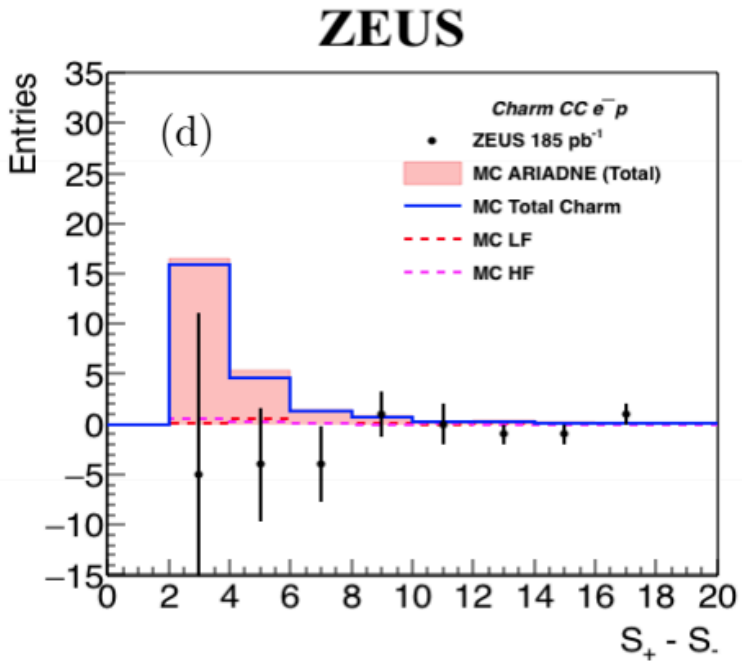

Requested for Paper

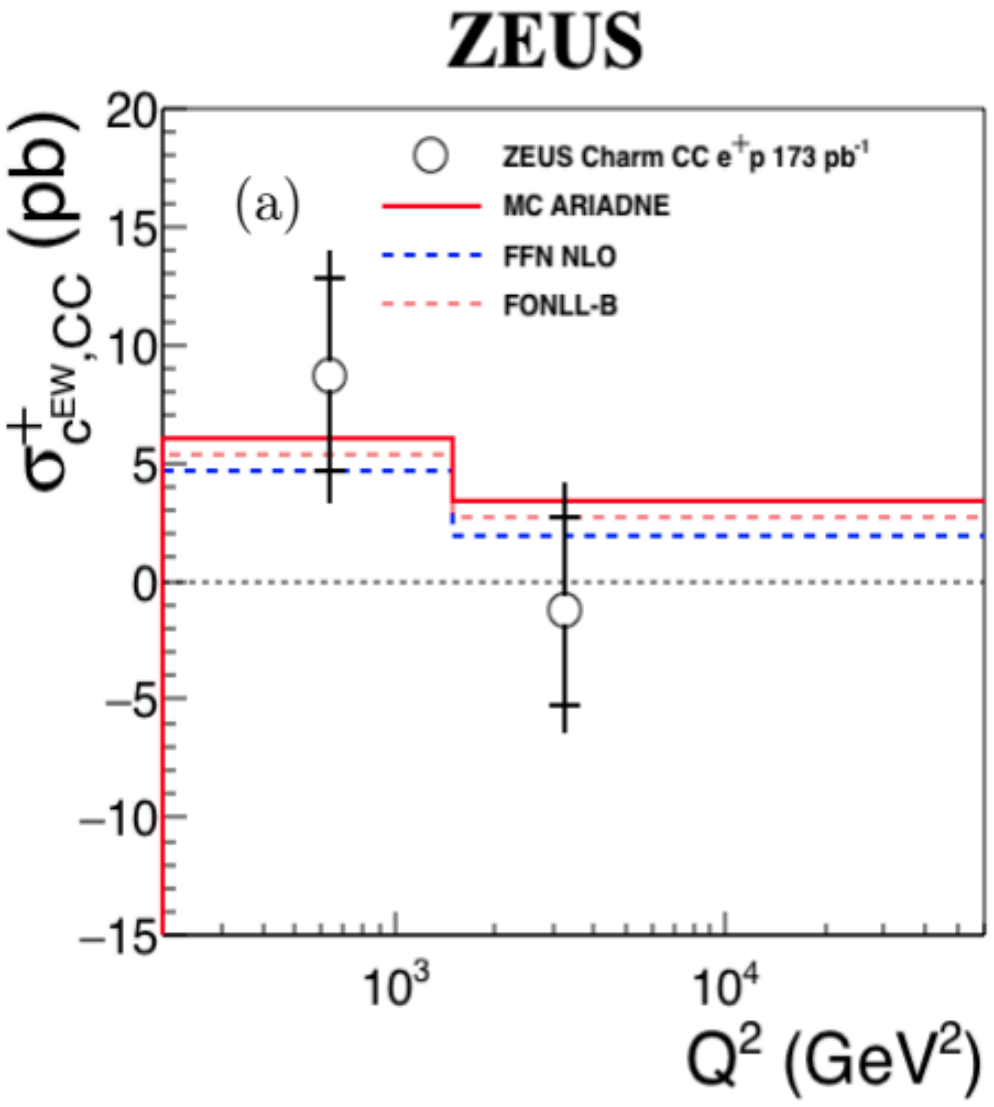

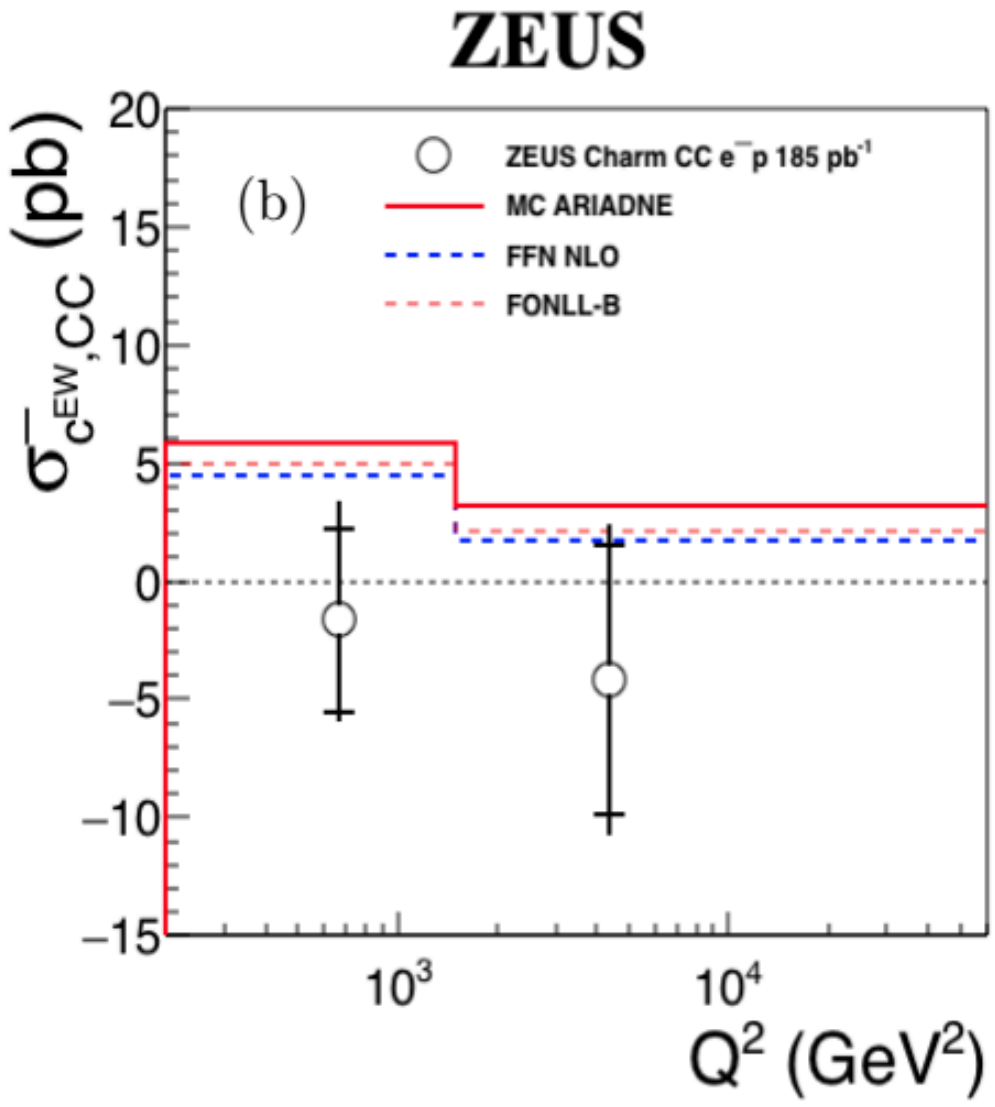

Back Up

Intermediate quantities

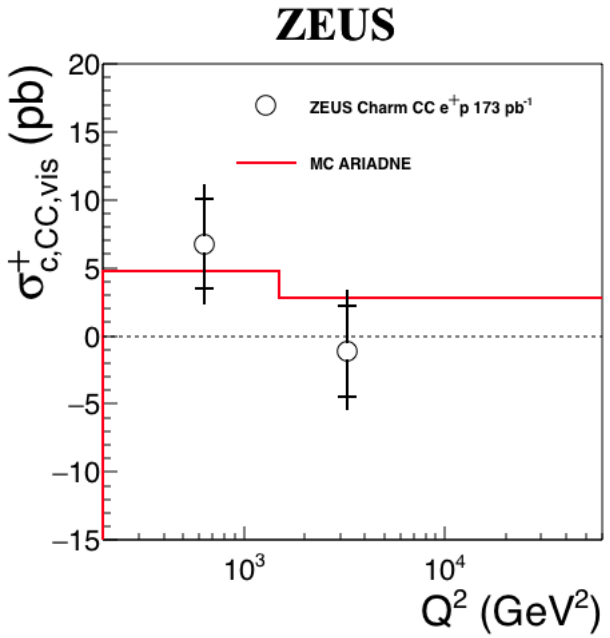

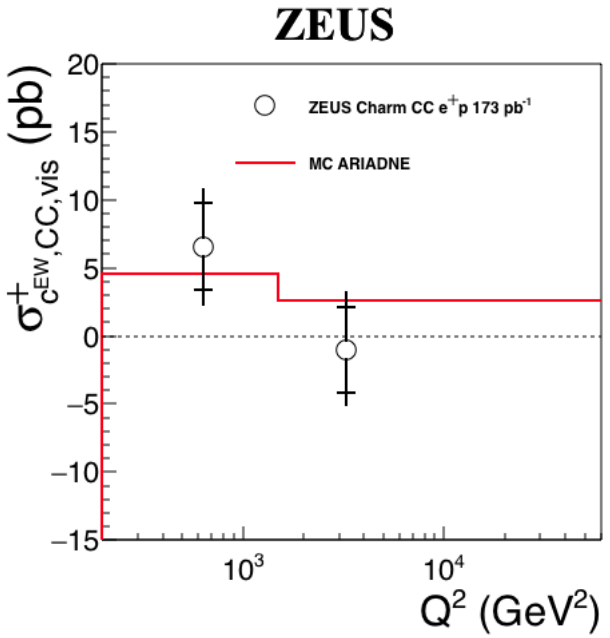

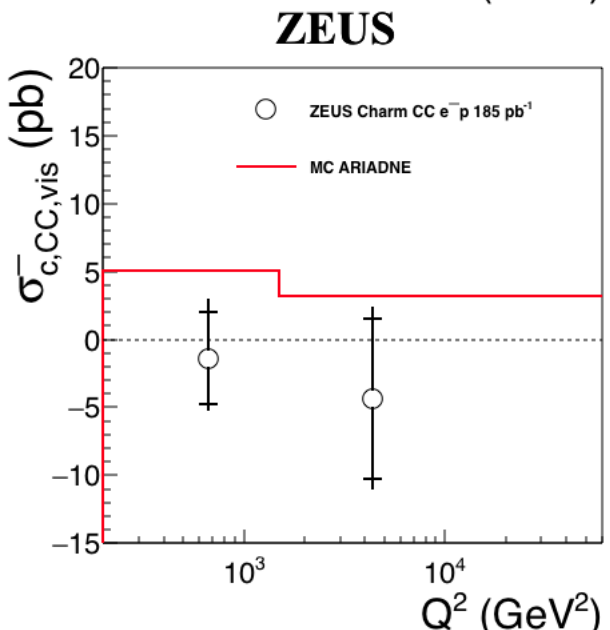

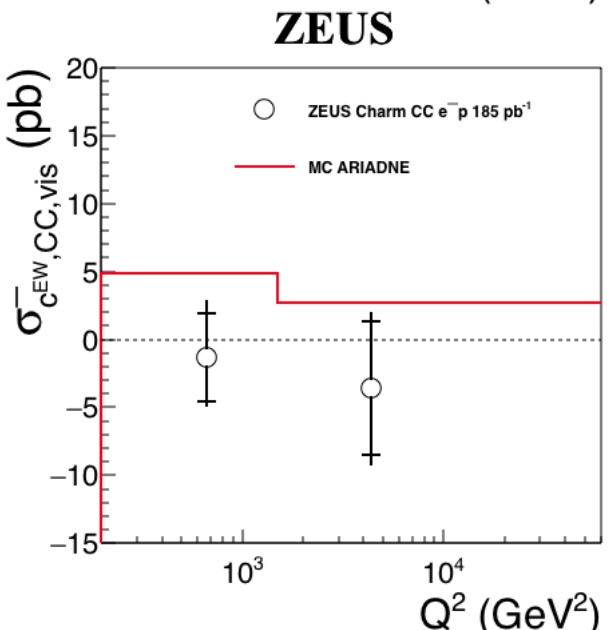

Determination of Significance Threshold

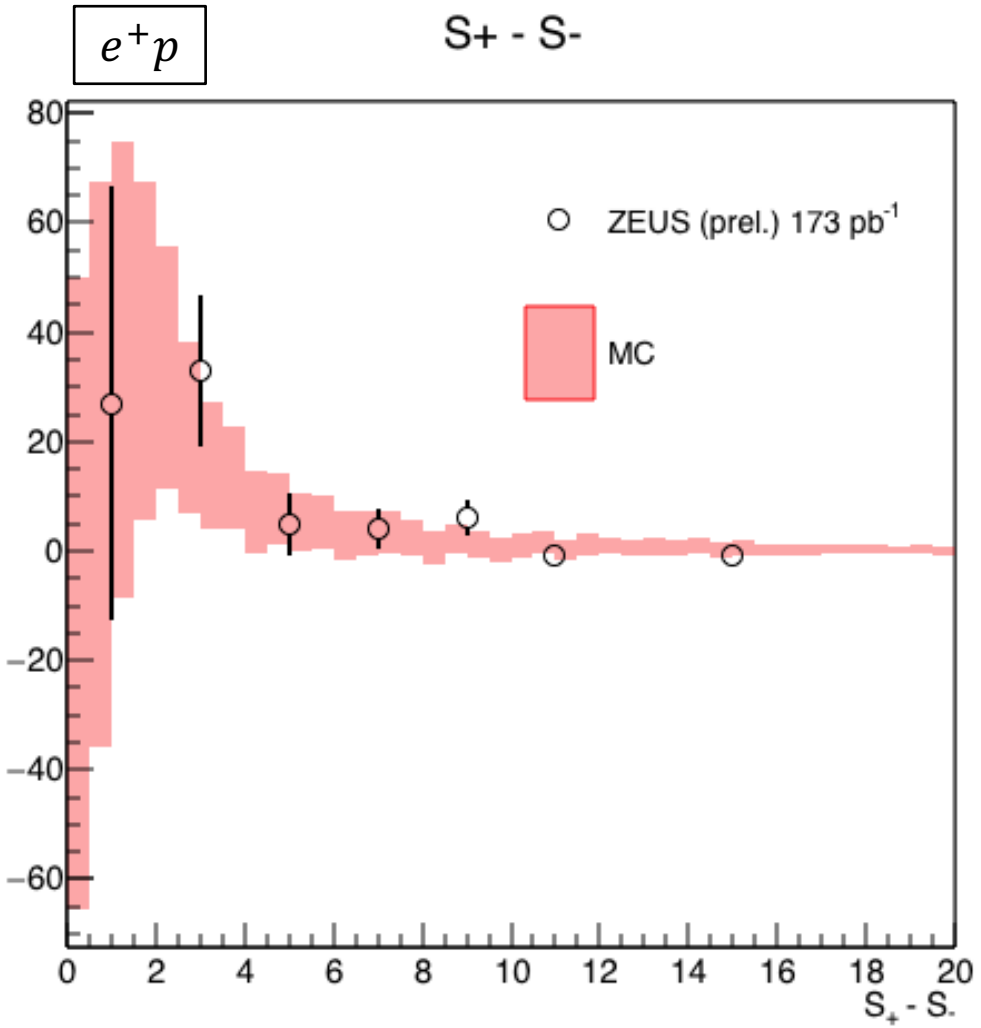

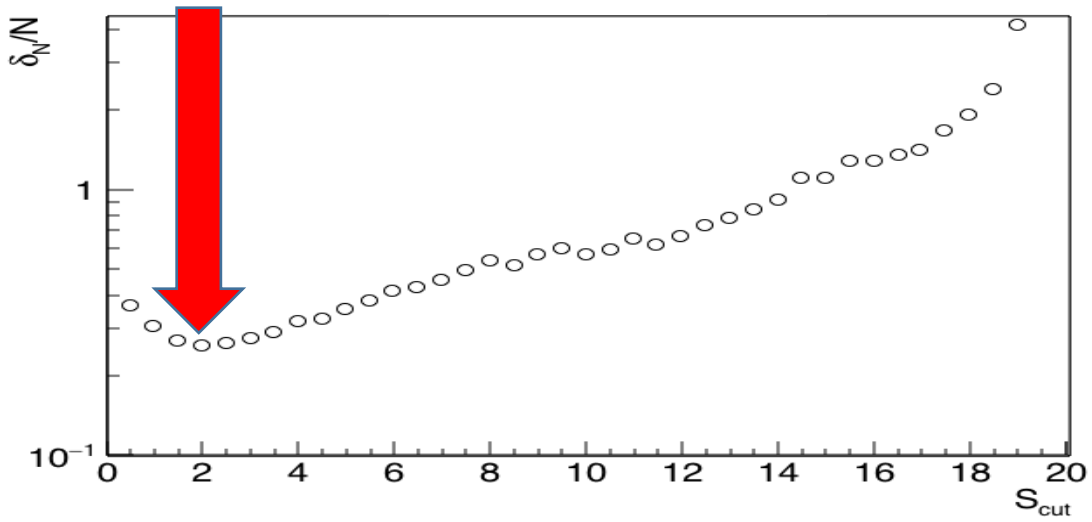

- The high symmetry and large statistics around $S \sim 0$ contributes to a large statistical uncertainty.
- A significance threshold cut was applied to reduce overall statistical uncertainty.
- From MC, the lowest δ/N is achieved if cut were to be applied at $S = 2$.

Determination of η^{jet} upper cut

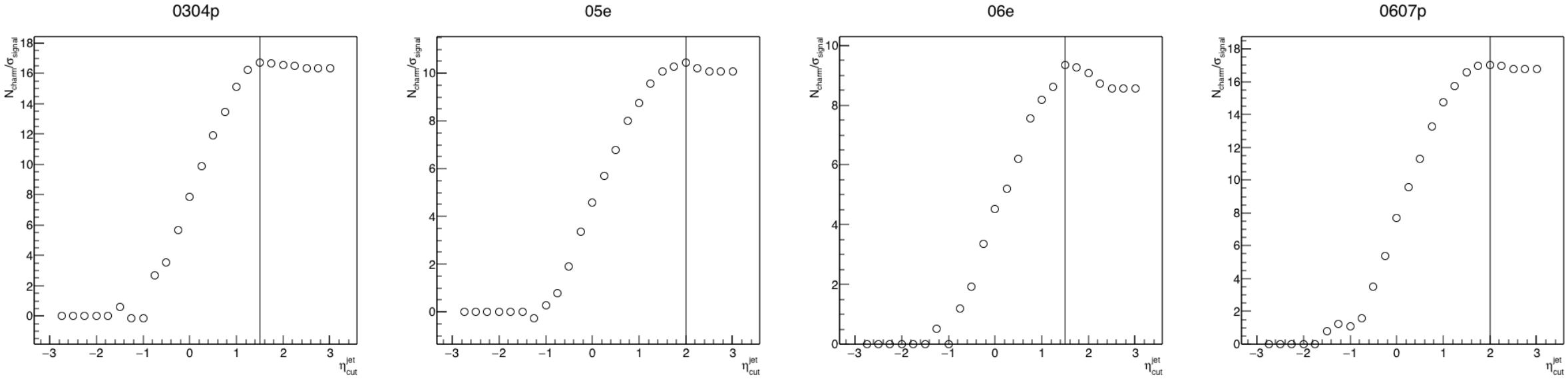

- $\frac{N_{charm}^{MC,mir}}{\sigma_{signal}^{MC,mir}}$ projected from MC as functions of η_{cut}^{jet} per different run period.
  - Highlighted in red vertical lines are the cut locations that would yield the highest ratio.

- In this presentation, $\eta^{jet} < 1.5$ for 05e (STT coverage), $\eta^{jet} < 2.0$ for else.
  - If not placed on the optimal position, the new η^{jet} cut will not reduce statistical uncertainty significantly.

Determination of N_{secvtx}^{trk} cut

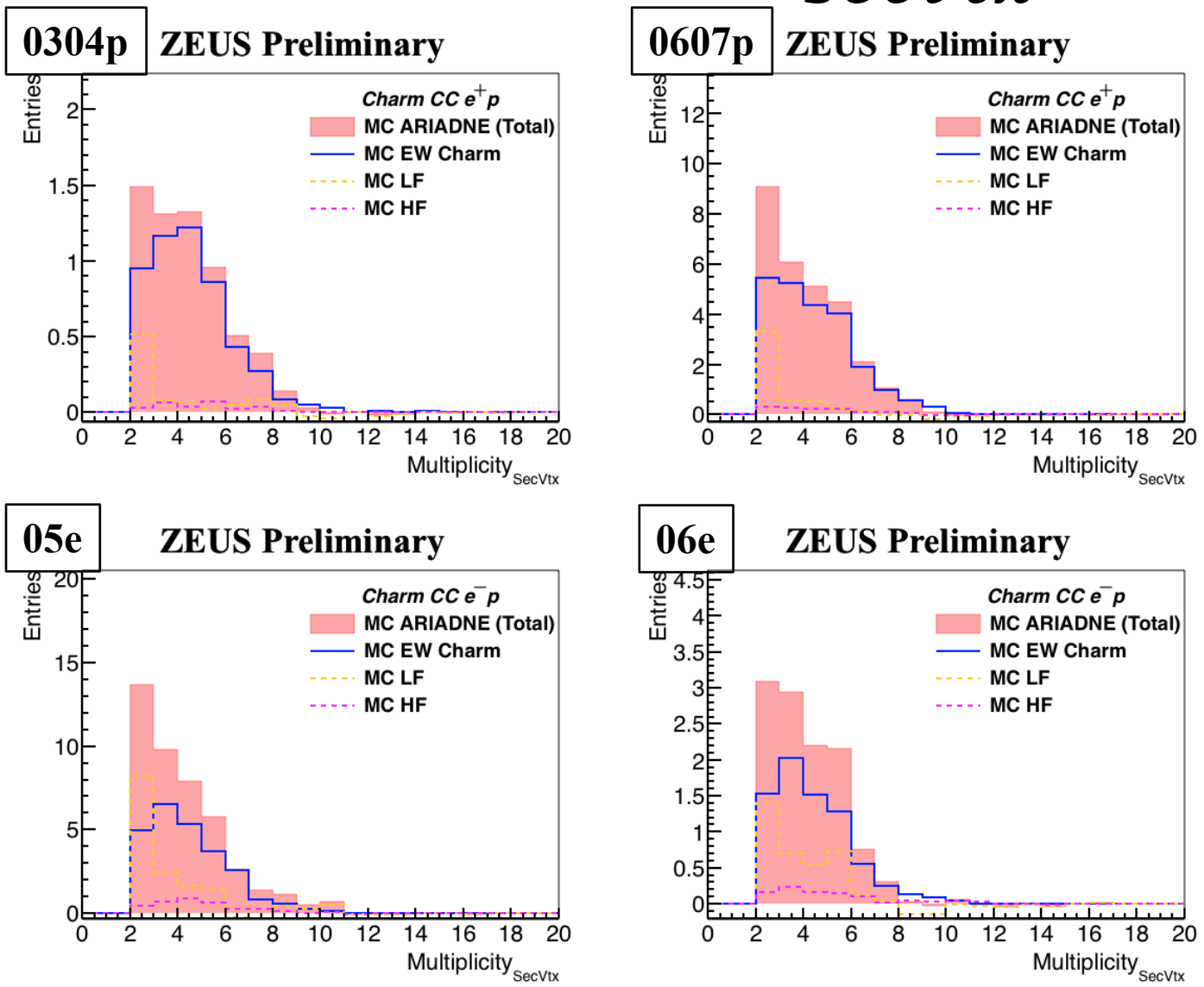

- A high concentration of LF background in low N_{secvtx}^{trk} region is observed across all run periods.
- A LF rejection cut was applied at $N_{secvtx}^{trk} > 2$.

Reconstructed variables

- Good agreement between True and Reconstructed Q^2

$$N_i = \sum_j C_{ij} M_j$$

$N_i = true\ number\ of\ entries\ in\ bin\ i$
$M_i = reconstructed\ number\ of\ entries\ in\ bin\ i$
$C_{ij} = correlation\ matrix\ element\ for\ bin\ i,j$

Collision	C_{11}	C_{22}
e^+p	0.99	1.01
e^-p	0.98	1.02

$e^+ p$

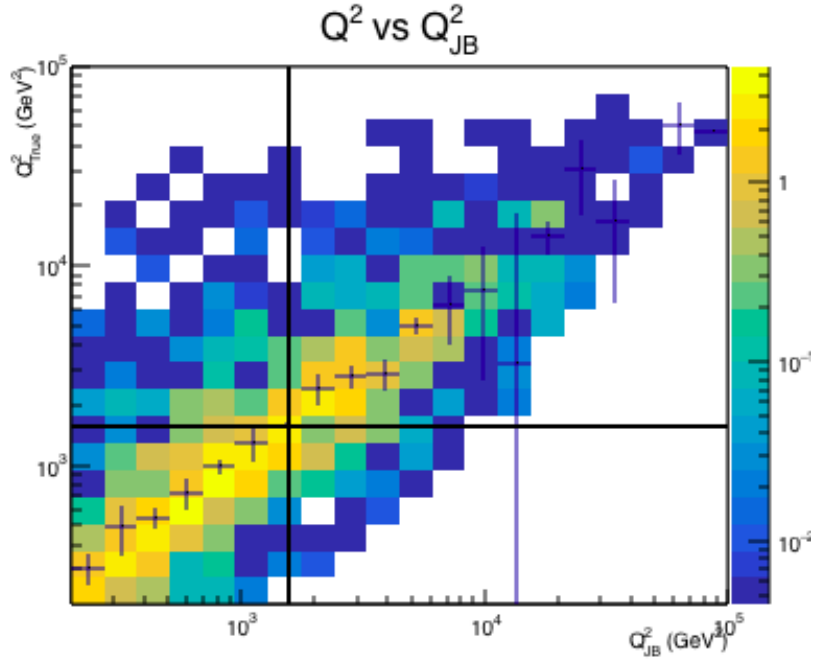

$e^- p$

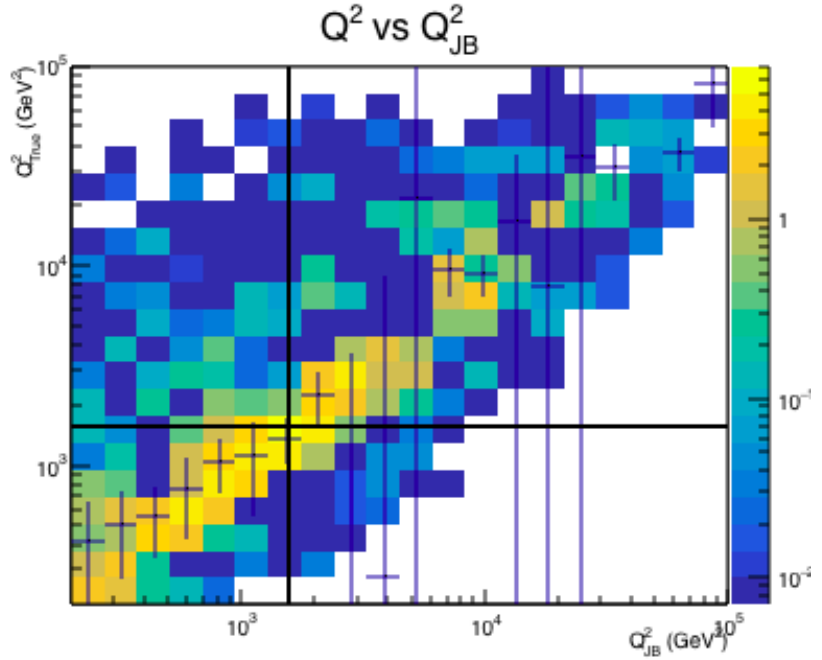

Uncertainty associated with signal ext.